



Norwegian University of
Science and Technology

Effect of filling pressure on Thermal Reignition Performance of free burning ultra-high Pressure Nitrogen arc

Shashidhara Basavapura Thimmappa

Master of Science in Electric Power Engineering

Submission date: June 2018

Supervisor: Kaveh Niayesh, IEL

Norwegian University of Science and Technology
Department of Electric Power Engineering



Norwegian University of
Science and Technology

Effect of filling pressure on Thermal Reignition Performance of free burning ultra-high Pressure Nitrogen arc

Shashidhara, Basavapura Thimmappa



June 2018

MASTER THESIS

Department of Electric Power Engineering
Norwegian University of Science and Technology

Supervisor: Kaveh Niayesh

Co-Supervisor: Fahim Abid

Abstract

The offshore power transmission system is developing fast due to growing demand for subsea electric power supply to oil and gas installations and increase in number of wind farms located far off from the coasts. As building platforms or floaters is too expensive, such offshore substations will be placed in seabed and its operations are controlled remotely. Electrical installations under seabed (i.e. switchgears using conventional technology either by gas circuit breaker or vacuum) should be designed with expensive solutions of encapsulation to protect them from high ambient pressure in seabed. A novel concept of filling the interruption chamber with seabed pressure can bring down the cost of encapsulation drastically. Furthermore, sulphur hexafluoride (SF_6) being a greenhouse gas with global warming potential of about 23,900 times to that of Carbon dioxide (CO_2). This has raised concern to reduce its usage drastically and even prohibition. This has led to effort in invention of alternative gas or gas mixtures by switchgear manufacturers and Research Institutes. Nitrogen (N_2) in supercritical state combines the benefits of both liquid and gaseous state. Current interruption characteristics of nitrogen at atmospheric pressure or at slightly elevated pressure have been studied so far, but remain unexplored in its supercritical (SC) state.

The aim of this thesis is to study the thermal reignition characteristics of the free burning arc in SC nitrogen medium. Rate of change of current before interruption and rate of rise of recovery voltage (RRRV) after interruption has been varied throughout the experiment.

To investigate the effect of pressure on reignition after current zero, the interruption chamber is filled with 3 different filling pressure. Resonant charging circuit using inductors and capacitors are used to apply the voltage across the electrodes before and after current interruption. This experiment is conducted at atmospheric pressure (1bar), 20 and 40 bar pressure. For simplicity, the scope of this thesis is limited to only free burning arc.

It has been observed that, filling pressure does not have a strong influence on the reignition in free-burning nitrogen arc. No clear improvement in reignition performance in supercritical state has been observed from the experiment. One of the reason behind such behaviour can be due to absence of active cooling mechanism in free burning arc.

Key Words: Arc discharges, free burning arc, current interruption, dielectric recovery, supercritical (SC) fluid, transient recovery voltage (TRV).

Acknowledgement

This master thesis report is a part of the two years International master program in Electric Power Engineering at NTNU. This experiment was conducted at 'High pressure current interruption lab' of SINTEF Energy Research in Tiller.

I would like to thank Prof. Kaveh Niayesh, supervisor of this thesis, for his technical guidance and valuable feedback throughout the master thesis experimental work. Fahim Abid, a Phd candidate in the same group is co-supervisor of this thesis, who helped in each step from day one to end of the experimental work. As this was continued part of his Phd work, he helped me understanding the experimental set up in detail. A significant part of the experimental works are based on the circuit used by him. Whenever I was looking for technical clarifications he guided me with valuable feedback. His support through out the thesis work has helped me complete my thesis in time. Special thanks to Mrs.Nina Sasaki Støa-Aanensen and Mr.Magne Runde for giving their timely help whenever needed.

Finally I would like to thank my parents, my wife, son and all of my friends for their continued support in pursuing my masters.

Shashidhara, Basavapura Thimmappa
Trondheim, June 2018

List of Symbols

f	Frequency [Hz]
j_o	Current density [A/m^2]
Ω	Electrical resistance [Ohms]
μ	Permeability [H/m]
ρ	Plasma density [electrons per unit volume]
σ	Electrical conductivity [S/m]
t	Time [s]

List of Acronyms

C	Celsius
CB	Circuit Breaker
HV	High Voltage
HVCB	High Voltage Circuit Breaker
IGBT	Insulated Gate Bipolar Transistor
K	Kelvin
kA	Kilo Ampere
kV	Kilo Volt
MV	Medium Voltage
N ₂	Nitrogen
P	Pressure
Pa	Pascal
RRRV	Rate of Rise of Recovery Voltage
SC	Super Critical
SCF	Super Critical Fluid
SF ₆	Sulphur Hexafluoride
T	Temperature
TRV	Transient Recovery Voltage

Contents

Abstract	i
Acknowledgement	ii
Symbols and Acronyms	iii
List of Tables	vii
List of Figures	x
1 Introduction	1
1.1 Problem Definition	2
1.2 Aims and Objectives	3
1.2.1 Aim	3
1.2.2 Objectives	3
1.3 Method	3
1.4 Main findings	4
1.5 Future work	4
1.6 Thesis disposition	4
2 Theory and literature review	5
2.1 High pressure arc	7
2.2 Thermal re ignition	7
2.3 Free burning arc	8
2.4 Ionisation mechanism in gases	9
2.5 Supercritical fluid (SCF)	11
2.6 Dielectric recovery experimental studies	12
2.6.1 Dielectric recovery study of SC Nitrogen	12
2.6.2 Dielectric recovery study of SC carbon dioxide	14
2.7 Experimental set up background	15
2.7.1 Test circuit philosophy	15
2.7.2 Ideal experimental setup	15

3	Experimental Setup	17
3.1	Experimental Simulations	17
3.1.1	Simulation by varying inductance value	18
3.1.2	Simulation by varying resistance value	20
3.2	Experimental Setup	21
3.2.1	Experimental procedures	30
3.2.2	Technical details of measurement devices	31
4	Experimental Results	35
4.1	Experimental data	35
4.2	Data processing	35
4.3	Case studies	39
4.3.1	For atmospheric(1 bar) pressure	39
4.3.2	For 20 bar pressure	43
4.3.3	For 40 bar pressure	47
4.3.4	For 1, 20 and 40 bar pressure	50
4.4	Discussion	53
5	Conclusions	54
5.1	Recommendations for Further Work	55
	Bibliography	56

List of Tables

- 2.1 Comparison of order of magnitude of properties for common insulating media in gas, liquid and Supercritical Nitrogen [17]. 12
- 3.1 For various inductance values. 18
- 3.2 For inductance value of 12 mH. 20
- 3.3 For inductance value of 44 mH. 20
- 3.4 For inductance value of 96 mH. 21
- 3.5 Test cases and values. 30

List of Figures

2.1	Schematic representation of switching arc and its various charge generation mechanism [9].	10
2.2	Phase diagram (p, V) for a pure compound in a close system. The triple point indicates the critical pressure and temperature of carbon dioxide [15].	11
2.3	Phase diagram of N ₂ in gas, solid and supercritical state [6].	13
2.4	Current and voltage wave forms of each gas-blast arcs from decaying to re-igniting [18].	14
2.5	Electron density of each gas-blast arc in the decay and re-ignition phases [18].	14
2.6	Reference test circuit [8].	15
3.1	Simulation of interruption current (di/dt).	18
3.2	Current and voltage waveform for 44 mH inductance.	19
3.3	Collapse of TRV during closure of switch S3.	20
3.4	Test circuit	22
3.5	Complete circuit set up in laboratory.	23
3.6	Circuit components mounted on table.	24
3.7	Circuit paths in laboratory setup.	25
3.8	Pressure vessel schematic [7].	26
3.9	Side view of Pressure vessel.	26
3.10	Inside chamber of pressure vessel.	27
3.11	Flange housing.	27
3.12	Measurement probes setup.	28
3.13	Control room setup.	29
3.14	Oscilloscope.	29
3.15	P6015A-1000X High Voltage Probe [23].	31
3.16	HVP 15HF High Voltage Probe [24].	32
3.17	LTX-5510R signal transmitter [25].	33
3.18	MSO 2024 Mixed Signal Oscilloscope [26].	34

4.1 Measured arc voltage and current at atmospheric (1bar) pressures and 30-mm electrode gap.	36
4.2 Measured arc voltage and current with filter at atmospheric (1bar) pressures and 30 mm electrode gap.	36
4.3 At TRV without filter.	37
4.4 At TRV with filter.	37
4.5 Typical data points for slope and current zero time period calculation.	37
4.6 Measured arc voltage and current with filtered wave forms at atmospheric (1bar) pressures and 30 mm electrode gap.	38
4.7 Current zero period and re ignition occurrence.	39
4.8 Delay in restrike (Δt) versus rate of change of current (di/dt) just before current zero at 1 bar pressure.	40
4.9 Delay in restrike (Δt) versus rate of change of TRV (dv/dt) after current zero at 1 bar pressure.	40
4.10 Breakdown voltage versus rate of change of current (di/dt) just before current zero at 1 bar pressure.	41
4.11 Breakdown voltage versus rate of change of TRV (dv/dt) after current zero at 1 bar pressure.	42
4.12 Delay in restrike (Δt) versus rate of change of current (di/dt) just before current zero at 20 bar pressure.	43
4.13 Delay in restrike (Δt) versus rate of change of TRV (dv/dt) after current zero at 20 bar pressure.	44
4.14 Breakdown voltage versus rate of change of current (di/dt) just before current zero at 20 bar pressure.	45
4.15 Breakdown voltage versus rate of change of TRV (dv/dt) after current zero at 20 bar pressure.	45
4.16 Delay in restrike (Δt) versus rate of change of current (di/dt) just before current zero at 40 bar pressure.	47
4.17 Delay in restrike (Δt) versus rate of change of TRV (dv/dt) after current zero at 40 bar pressure.	47
4.18 Breakdown voltage versus rate of change of current (di/dt) just before current zero at 40 bar pressure.	48
4.19 Breakdown voltage versus rate of change of TRV (dv/dt) after current zero at 40 bar pressure.	49
4.20 Delay in restrike (Δt) versus rate of change of current (di/dt) just before current zero 1, 20 and 40 bar pressure.	50

4.21 Delay in restrike (Δt) versus rate of change of TRV (dv/dt) after current zero at 1, 20 and 40 pressure.	51
4.22 Breakdown voltage versus rate of change of current (di/dt) just before current zero at 1, 20 and 40 bar pressure.	52
4.23 Breakdown voltage versus rate of change of TRV (dv/dt) after current zero at 1, 20 and 40 bar pressure.	52

Chapter 1

Introduction

Electrical switchgears in power system networks are responsible for the protection of the power system components and the control of the power flow. These switches are dis-connectors, earthing switches, load break switches and circuit breakers. Circuit breakers are capable of breaking or making normal load and short circuit current in the network. Circuit breakers must interrupt the current quickly, and regain the dielectric strength rapidly after the interruption, especially in high voltage circuit breakers (HVCBs). In other words, a high dielectric strength and a fast dielectric recovery speed are the two vital characteristics of such circuit breakers.

New renewable energy wind farms are being installed far away from the coast for power generation. Also, offshore production of oil and gas at deeper waters has been challenging and for efficient and secure production, processing facilities are being installed at deep ocean floors. Pressure at depth of 3000 meter or more is found to be around 300 bar or more. The switchgear designed for such application should be capable of handling such high pressure at seabed. This has led to the investigation of the design of switchgear at high pressures, which can reduce encapsulation costs [1].

At present SF₆ switchgears are dominating in terms of installations and operations in MV and HV switchgear application due to its electronegative nature and exhibiting good dielectric insulation properties. However, it is a greenhouse gas and its usage at present is highly restricted and may be prohibited in near future. This has led to many technical institutions and switchgear manufacturing company research divisions to work on the possible alternative solutions to replace present SF₆ technology. There are already some gas or gas mixture solutions which have been experimented, tested, installed and are under observation for their reliable functionality [2].

Successful interruption of the switchgear depends on how effectively and efficiently the heat

from the arc channel is taken out (by cooling of the arc channel) after current zero, and on how fast the medium regain dielectric strength to avoid restriking [3]. The post arc dielectric strength of the insulation medium must always be higher than the transient recovery voltage developed according to race theory. Electrical switching equipment's are expected to interrupt the fault current without failure. It is vital to make sure that even in highest possible fault current interruption in network, the dielectric medium in switchgear should be capable to interrupt the fault current without any re strikes. As a result the dielectric recovery characteristics of commonly used gases at atmospheric pressure or slightly high pressure (up to 10 bar) is well explored [4], [3] and [5].

Nitrogen is the major component of the Earth's atmosphere and hence it has no environmental impact. Nitrogen, when subjected to high pressure above the critical point at room temperature, enters into supercritical state. In this state it is found to be exhibiting good dielectric properties. The existing investigative studies have shown satisfying dielectric strength of nitrogen in SC state. However, there are not so much work in the past related to very high pressure arc beyond supercritical state. Existing studies about the breakdown voltage inside SC nitrogen have proven satisfying dielectric strength at SC state under low energy deposition [6]. The study design consists of SC plasma switch for pulsed operation in repetitive mode (200 ns pulse duration and 10–1000 Hz pulses per second) at pressure of 32–95 bar [6]. However, these studies are mainly limited to spark type discharge and for very low energy dissipation. In circuit breaker application, very high energy is deposited in the arcing channel. Hence, there is a need to understand the post arc thermal and dielectric recovery characteristics of high energy arcing channel. Dielectric recovery studies with Carbon dioxide, Perfluoroketone, Perfluoronitrile, Trifluoridomethane as insulation medium and vacuum technology have also been investigated. The dielectric recovery characteristics in SC nitrogen has been already studied using SC nitrogen blown plasma switch [6]. However, both thermal and dielectric recovery of post arc phase in nitrogen for arc current (high energy deposition) needs to be studied.

1.1 Problem Definition

The arc voltage characteristic of nitrogen at supercritical state have been investigated recently [7]. However, thermal reignition and dielectric restriking characteristics of free burning arc after current zero in nitrogen filled chamber at high pressure is yet to be studied. This thesis is limited to the effect of filling pressure on the thermal reignition performance of free burning ultra-high pressure nitrogen arc (including supercritical state).

1.2 Aims and Objectives

This section discuss about the aim and objective of the master thesis in brief.

1.2.1 Aim

The aim of this master thesis is to study post arc thermal reignition performance of free burning arc in nitrogen chamber at atmospheric, 20 and 40 bar pressures using passive RLC circuit which can control the rate of change of current before current zero and rate of rise of recovery voltage after current zero.

1.2.2 Objectives

The main objectives of this thesis are

- Literature review on present research studies on this topic and choosing a suitable method to investigate the post arc thermal reignition performance.
- Simple simulation of the behaviour of the circuit in order to understand the circuit.
- Preparation of laboratory circuit to conduct experiments.
- Data collection for varied rate of rise of recovery voltage and varied current slope near current zero at different filling pressure.
- Data analysis and finding the correlation between "re-ignition time" and "voltage when re-ignition occurs" with respect to different di/dt near current zero and dv/dt [RRRV] with different filling pressures.

1.3 Method

The methodology is based on the fact that the initiation of a thermal re-ignition depends on the rate of increase in initial TRV to its peak value [8]. This study is done for different pressure values in a closed nitrogen filled pressure vessel. Ignition wire is tied between copper-tungsten electrodes, where the copper-tungsten electrodes are separated at fixed distance. The rate of change of current (di/dt) near current zero is varied by changing the circuit parameters. The circuit can also vary the slope (dv/dt) of the TRV applied after current zero. The time taking to re-ignite the arc and the voltage when the re-ignition occurs are considered as the main parameters to characterise the post arc thermal reignition dielectric performance at different filling pressure levels.

1.4 Main findings

It has been observed that the re-ignition time decreases with high di/dt and high dv/dt , which is expected. However, the pressure dependency on re-ignition time and the re-ignition voltage is not strong. This is probably due to the fact that in free burning arc, no active cooling mechanism is present.

1.5 Future work

- Further investigation on actively cooling arc, such as puffer/self blast techniques was beyond the scope of this thesis, and hence not included here. However this can be a future work.
- Use of triggering and time delay units to control delay time after current zero for further precise study of re-strike performances.
- Use of high speed camera to study re-ignition after current zero will be quite interesting.
- Use of high value capacitors in the circuit can produce high current amplitude. This study was conducted in the frequency range of 230 Hz-350Hz. Thus post arc current behaviour can be studied for practical grid current rating near to power frequency.

1.6 Thesis disposition

This report consists of five chapters. Chapter 1 of the report discusses brief overview about the purpose, aims and objectives, main findings, future work of the thesis and overview of the report structure. Chapter 2 includes brief literature review which consists of theory and findings of the previous studies carried out related to thesis topic. This gives good foundation to achieve the objectives of the thesis. In chapter 3 simulation circuit and results were presented to estimate the expected result in laboratory experiment. Also, includes description of experimental setup and methodology based on the literature review. Experimental results for different case studies and interpretation of the experimental outcomes are covered with discussion in chapter 4. Finally chapter 5 consists of conclusions drawn based on the experimental results and suggestions for future work.

The chapters of the report is subdivided in such a way that the reader can easily follow the objectives, previous works, methodology and the findings of the thesis with minimum background on the topic.

Chapter 2

Theory and literature review

Electrical switchgears during making and braking operations experience thermal, mechanical and dielectric stresses. The dielectric medium is expected to withstand the stresses developed. The extinguished arc between the contacts will have charged ions and electrons which result in reduction of the dielectric strength of the medium [9].

Transient recovery voltage drives a post-arc current through the remains of the decaying arc plasma immediately after current zero which results in a heating effect. The energy balance between this heating and cooling effects either results in a decay of the plasma and an interruption of the current, or in a reheating of the gas to a well-conducting arc column, this is known as thermal re-ignition [10]. The thermal recovery depends on the circuit parameters, contact material properties, arc chamber design geometry, transient recovery voltage values and current value [4].

Arc current: Higher amplitude of the arc current, higher becomes the arc temperature and the density of electric charge carriers generated in the arc. The Steeper the di/dt , less the time period to change from conducting to insulation state.

The slope of the interruption current before current zero is an influencing parameter to determine if the re-strike is likely to occur or not. If the slope, di/dt is high during this time the residual charged electrons are active in the region which needs efficient cooling to avoid any further re strikes. If the cooling is not sufficient, then thermal ionisation will further lead to high possibility of the occurrence of the reignition. On the other hand, if the current slope rise is gradual and more the time period of the current slope more time the charged electron get to cool down. This will lead to successful arc quenching without any further re-strikes [9].

The exact time the contacts separated defines the arc time. If separation happens just before

the current zero, then the current will continue to conduct for one more cycle (typically in the range of 0.5–1.5 times the length of a current half cycle) before interruption. This occurs because the opening mechanism in switchgear is random variable. This will result in increased energy dissipation [9]. The arc voltage depends on influence of current, arc length, pressure in arcing chamber and arcing medium in the switchgear. The higher the arc voltage, higher is the energy deposition in the arc.

Transient recovery voltage (TRV): Energy oscillations between the energy storage elements in the network are vital in determining the transient recovery voltage developed across the contact terminals. The TRV to which a circuit breaker is subjected depends on the type of fault, the location of the fault and the type of circuit switched. When successful current interruption occurs (after current zero crossing), transient voltage is developed across the contacts. This voltage can accelerate the remaining electric charge carriers present in the contact gap, increasing the chance of getting charge carrier multiplication by impact ionisation and finally lead to a breakdown of the switching gap and formation of a new arc. Thus, the TRV is one of the key factors determining switching device ability to interrupt a current [9].

$$\text{Energy dissipated} = F(t) = \int_{t \text{ separated}}^{t \text{ closed}} u_{\text{arc}} i_{\text{arc}} dt \quad (2.1)$$

During conduction of arc, residual charges will be active in the arc path. If the cooling is insufficient then the conduction of the residual charges may re-ignite the arc path. Thermal re-strike occurs immediately (up to a few microseconds) after current zero and is greatly dependent on the recovery voltage shape, especially its steepness, during this period. If the current interruption is successful due to efficient cooling then the voltage across the contacts increases. If this voltage is more than withstand strength of the dielectric medium then the dielectric re-ignition will occur. Often it is found that the most critical time as to whether a dielectric re-strike will occur is a few milliseconds after current zero. Thus, the possibility of having a dielectric re-strike is influenced by the shape and amplitude of the recovery voltage in this period [9].

During breakdown the insulation medium switches from being insulator to a good conductor state. This is due to generation of large number of charge carries as electrons and ions. These charge carriers are generated either from electron emission from electrodes or by ionisation of the gas molecules. The later phenomenon is assumed to be the main cause of free charge carriers in gas circuit breakers. The ionisation in gases occurs due to electron impact (impact ionisation) [9].

2.1 High pressure arc

In this thesis, we are working mainly with high pressure arc and it can be explained as the charged particles responsible for current flow after opening the contacts are mainly produced by thermal ionisation of the gaseous medium. The charged particles are accelerated by the electric field within the arc, and due to their motion a current is generated. The current flowing through the arc determines the energy dissipated in arc path. The dissipated energy partly contributes to the temperature increase of the plasma. Efficient cooling is necessary to change the temperature instantaneously. If the cooling mechanisms are so efficient that much larger amounts of power are drawn out of the arc than generated by the current flow, the temperature and consequently the conductivity of the medium decrease, which results in successful interruption of current [9].

The electrical conductivity of the arc is highly dependent on the arc temperature and cross-section. The temperature distribution in arc column depends on current value. For low currents the arc temperature changes in line with changes in the current, whereas at large currents the maximum temperature is fairly constant across the cross-section [9].

2.2 Thermal re ignition

During the arcing period, the breaker gap is subjected to high temperatures and will have high electrical conductivity. It is during this recovery period that the circuit re-striking voltage is applied. Any further arc reignition occurrence depends upon the reaction between the applied voltage and its conductive effects and process of recovery. Past experience shows that the main modes of reignition are via spark breakdown, glow-to-arc transition and thermal breakdown. The study results show that, in the early post-arc period, reignition is via thermal breakdown. Further, reignition occurs via a spark and glow-to-arc transition at the electrodes, and finally the recovery reignition is by pure spark breakdown [11].

Most of failures occur in gas circuit breakers originate from a soft thermal collapse of the gas insulation within less than microsecond after current zero [8]. This thermal re ignition occurs mainly because of the post arc plasma left between electrode arc path. Further the post arc current flow due to application of TRV will increase conductivity of the rest plasma due to high speed of the remaining charged particles in the applied electric field. The density of the rest

charged particles depends on the rate of fall of current before current zero. Also, depends on post arc current produced due to post arc applied voltage. It can be concluded that the thermal re ignition is strongly dependent on the rate of decrease in the current before current zero as well as on the rate of increase in the recovery voltage [8].

It is also seen from the experiment that during period immediately following the interruption of a thermionic arc, the gap behaves as a transient resistor and that during this period the concept of thermal reignition is applicable [11].

2.3 Free burning arc

Theoretical understanding of free burning arc is simple as in contrast to forced cooling cases (ablation/puffer type). We limit it to a special case and the arc is not affected by outside parameters like mass flow or ablation amount, ablated material etc.,

The intensity and properties of arc mainly depends on arc current value. Firstly, at low currents of typically below 30 A, the controlling physical process is natural convection. Secondly, at higher current (up-to 20,000 A) the properties are determined largely by convection and also with self-magnetic field of the arc as self magnetic field is very dependent on the current flow [12].

The arc current in this thesis is 250 A, which comes under high current region. The theoretical equations developed for high current arc for vertical electrode set up at distance of 1cm at atmospheric pressure (air) performed under few approximations are mentioned from the works of J.J.Lowke [12].

$$R = 1.11(z/h\sigma)^{\frac{1}{4}} I^{\frac{3}{8}} / (\mu j_0 \rho)^{\frac{1}{8}} \quad (2.2)$$

$$E = 0.26(h/z\sigma)^{\frac{1}{2}} I^{\frac{1}{4}} / (\mu j_0 \rho)^{\frac{1}{4}} \quad (2.3)$$

$$V = 0.52(hz/\sigma)^{\frac{1}{2}} I^{\frac{1}{4}} / (\mu j_0 \rho)^{\frac{1}{4}} \quad (2.4)$$

Where, E is electric field, V is arc voltage, R is arc radius (in cm), z is axial position (in cm), ρ is density of plasma, σ is electrical conductivity and h is enthalpy of plasma, μ is permeability of the material and j_0 is current density. Our thesis work the electrode distance is 3cm the accuracy of the derived values in above equations are still valid. For values of z above few cm the inaccuracy increases due to viscous and turbulence effects [12].

pressure dependency: The value of ρ is approximately proportional to pressure value p . Considering the current density independent of the pressure, the equations 2.2, 2.3 and 2.4 will give

$$R \propto p^{\frac{1}{8}} \quad (2.5)$$

$$E \text{ and } V \propto p^{\frac{1}{4}} \quad (2.6)$$

In high pressure arcs, thermal ionisation is the most important charge generation process. Impact ionisation can be of relatively greater importance near current zero crossing. Ionisation due to radiation plays normally only a minor role [9].

2.4 Ionisation mechanism in gases

Ionisation process is observed in the dielectric medium soon after the electrical breakdown occurs in interruption chamber. They are like ionisation waves observed as luminous fronts. These waves travel with velocity depending upon the defined experimental conditions.

For homogeneous electric field where velocity of ionisation is governed only by electron drift, the ionisation waves travel with relatively low propagation velocities of range 10^5 to 10^7 cm/sec. In this stage current associated will be low of the range of tens of ampere due to heavy particle participation in ionisation process. During the final stage of the electric breakdown where plasma exist, the ionisation waves travel at subluminal velocities of range 10^8 to 10^{10} cm/sec. Here the current associated will be high of tens and hundreds of kilo amperes. It is also possible to have velocity of the ionisation waves to reach from 3×10^8 to 2×10^{10} cm/sec (for voltage amplitude increase from 60 to 300 kV in this time period) provided there occurs sharp rise in TRV slope. Shorter the applied voltage pulse and the stronger the pre-ionisation of the discharge gap. The current transported is so high that discharge gap will breakdown at first passage of wave itself [13].

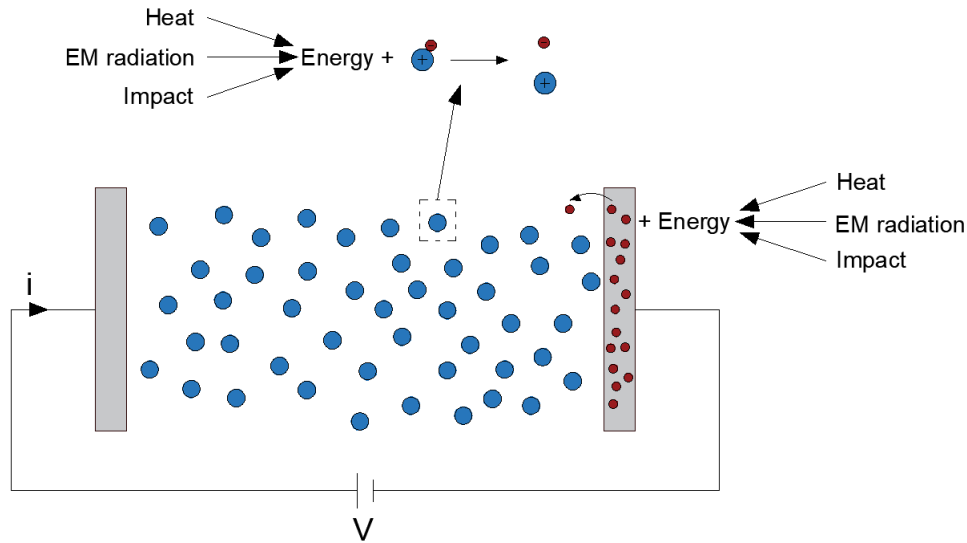


Figure 2.1: Schematic representation of switching arc and its various charge generation mechanism [9].

Thermal ionisation: In this process due to increased temperature the dissociation of the molecules occurs in gases. Eventually this will result in more and more free electrons and positive ions generation by detaching from their atoms.

Thermal ionisation can be correlated to the basic kinetic energy formula as below [9].

$$W_k = \frac{1}{2} m v^2 = \frac{3}{2} k T$$

Where m is mass, v is mean value of velocity, k is constant and T is temperature of gas molecule.

Impact ionisation: The impact ionisation occurs when the free electron energy is equal or greater than the ionisation energy of the particle it collides with [9].

Electron emission: Metal electrodes consists of free electrons. These electrons get energy due to thermionic emission or reduction of distance between electrodes or by application of high electric field. This phenomenon can finally result in current flow or arc formation. In most cases it is cathode which which active and supplies the electrons to the arc column [9].

2.5 Supercritical fluid (SCF)

It is known that particles in solid are rigid, have fixed shape and fixed volume. When solid (e.g., ice cube) is heated it melts into liquid losing its rigidity and shape but volume still remain fixed. After heating it beyond boiling temperature it turns in liquid which is not rigid, no shape and no fixed volume. The density will be like liquid and viscosity as gas. Heating a liquid above boiling conditions causes vapour bubbles. But heating a supercritical fluid does not cause vapour bubbles. This property along with high heat capacity and high heat conductivity is the important property for application in high voltage [14].

Molecules distribution in all the states of the gas mixture along with SC state of Carbon dioxide is shown in the figure 2.2 [15].

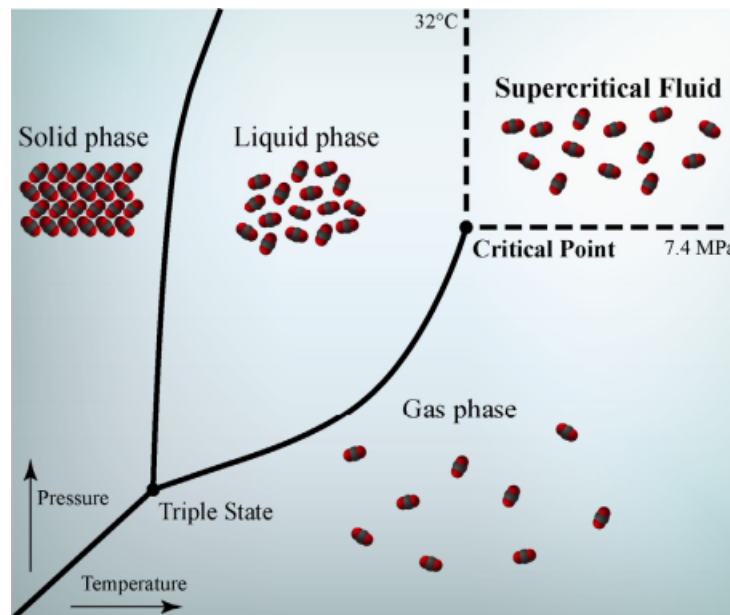


Figure 2.2: Phase diagram (p, V) for a pure compound in a close system. The triple point indicates the critical pressure and temperature of carbon dioxide [15].

Super critical fluids exhibits the following characteristics, which are believed to be suitable for it to be used as dielectric medium in high voltage switchgears [16].

- They exhibit high values for thermal conductivity and specific heat.
- Viscosity is proven less compared to liquid but higher than gas.
- They possess superior transport and dissolution attributes.

- The dielectric strength is high compared to liquid or gaseous state.

Break up study in liquid nitrogen jet grow at sub-critical pressure shows acting surface tension is clearly reflected in the formation of small distinct droplets and sharp interfaces. As pressure increases to supercritical value then the surface tension drastically reduces to negligible amount and no sharp interfaces can be identified. According to the study it has been observed that, there is not only state called as supercritical fluid, but within supercritical fluid present two distinct state as liquid and gas. Transition occurs from liquid to gaseous state. The molecular distribution remains virtually indistinguishable irrespective of pressures between liquid and transcritical states [16].

The below table 2.1 gives comparison of order of magnitude of properties for common insulating media in gas, liquid and SC N₂. The value of diffusivity is the order of magnitude figure for N₂ in range of T=70-500 K, p=0.1-80MPa [17].

Table 2.1: Comparison of order of magnitude of properties for common insulating media in gas, liquid and Supercritical Nitrogen [17].

	Density	Viscosity	Diffusivity	Heat capacity	Thermal conductivity
	[kg/m ³]	[μPa.s]	[m ² /s]	[10 ⁶ J/m ³ /deg]	[10 ⁻³ J/m/s/deg]
Gas	1	10	10-300	1	20
SC N ₂	100	50	2-60	100	100
Liquid	500	100	1-2	500	200

2.6 Dielectric recovery experimental studies

2.6.1 Dielectric recovery study of SC Nitrogen

The figure 2.3 shows the N₂ covering pressure up to 20 MPa, temperature in the range 86–306 K [12]. P_c = 3.3958 MPa and T_c = 126 K represent the critical pressure and temperature of N₂, respectively [6].

An experimental and numerical modelling of the dielectric recovery of SC N₂ has been studied [6]. The study is done for gap distance of 0.2 to 0.45 mm which is very small compared to industrial application circuit breaker contact distances for high voltages. Special plasma switch has been designed for testing. The test circuit uses pulsed voltage as input and voltage is amplified by four times by transmission line transformer before applying to SC plasma switch. The post breakdown recovery characteristics shows expected result as pressure and distance between contact increases the dielectric strength increases [6].

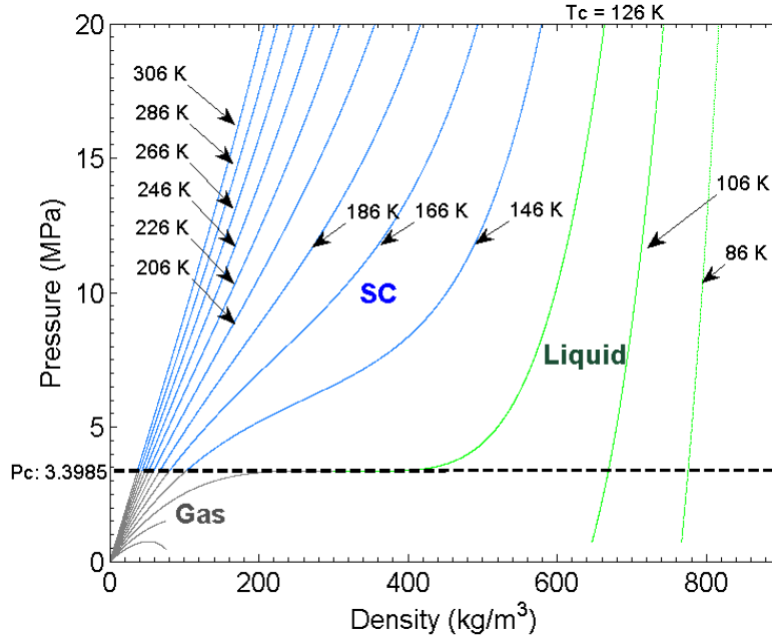


Figure 2.3: Phase diagram of N₂ in gas, solid and supercritical state [6].

The study on thermal re-ignition processes of switching arcs with gas-blast in nitrogen chamber using TRV application by power semiconductors has been carried out. Here the investigation of fundamental aspects of both decaying and re-ignition processes of gas-blast arcs along with electron density measurement were carried out. The gas chamber was filled with pressure of 0.1 Mpa and arc current of 50 A was applied. The distance between electrodes is 50 mm (full open position of electrode). At $t = 20 \mu\text{s}$, a quasi-TRV with a RRRV of $1.7 \text{ kV}/\mu\text{s}$ was intentionally applied between the electrodes in this case. The result shows the arc current and arc voltage decreased to 0 V and 0 A in $5 \mu\text{s}$ from the initiation of arc decay. By application of the quasi-TRV to the N₂ residual arc, the arc re-ignition occurred at 0.35 kV as shown in the figure2.4 [18]. For arc quenching phenomena, the electron density is a key parameter which determines the electrical conductivity in thermal mode and electron avalanche in dielectric mode. The N₂ arcs have higher electron densities around $10 \times 10^{22}/\text{m}^3$ at $t = 0 \mu\text{s}$. This electron density decays with time monotonously. At $t = 10 \mu\text{s}$, it reached to $4.6 \times 10^{22}/\text{m}^3$. The electron density is $1.8 \times 10^{22}/\text{m}^3$ at $t = 20 \mu\text{s}$. This value is similar to those in SF₆ and CO₂ at $t = 20 \mu\text{s}$. After the arc re-ignition, the electron density is elevated to $8 \times 10^{22}/\text{m}^3$ until $t = 30 \mu\text{s}$ as indicated in figure 2.5 [18].

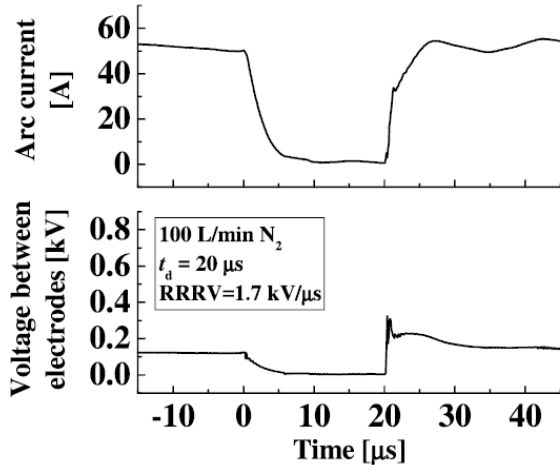


Figure 2.4: Current and voltage wave forms of each gas-blast arcs from decaying to re-igniting [18].

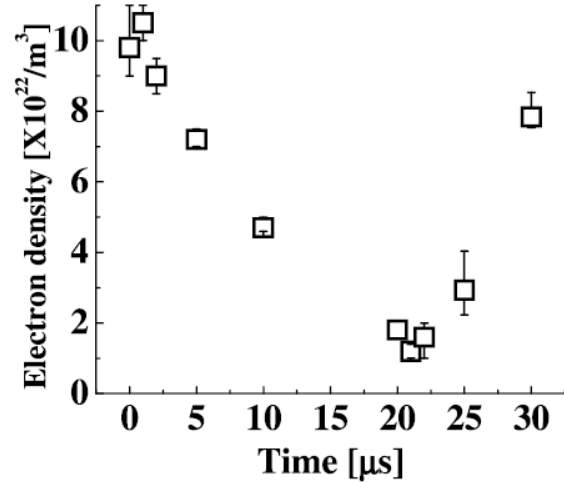


Figure 2.5: Electron density of each gas-blast arc in the decay and re-ignition phases [18].

Though the experimental set up and parameters in our study is different, nevertheless above mentioned previous work gives good understanding about the nature of arc in nitrogen chamber.

2.6.2 Dielectric recovery study of SC carbon dioxide

Discharge study at very high pressure CO_2 have been conducted to measure its behaviour at different electrode distance. The experimental set up is simple with SCF cell (along with pressure inlet and outlet arrangement) with dc power source, sensors and controllers. The contact electrodes were fixed platinum plates with thickness and width of 0.1 mm and 5 mm. In this study the breakdown voltage is tested for contact distance of 1 and 2 μm . Results shows that the breakdown voltage in later is higher (more than 1.5 times) than former one.

The results reveal an inflection near 2.5 MPa and breakdown voltage channel near the critical point and show that an ionised state or plasma state in a SCF environment can be generated with very low voltage. Further, the densities of ions and electrons in a SCF environment might be very high, since, as revealed by series of experiments on micro/nano meter scale plasma, the densities of ions and electrons become higher due to the higher permissible particles [19].

2.7 Experimental set up background

2.7.1 Test circuit philosophy

The experimental circuit built in this thesis is based on the test circuit as shown in figure 2.6. The main objective of this circuit is to apply the recovery voltage with reduced amplitude but with same rate of rise of voltage (dv/dt) within the first microseconds after current zero to the test circuit breaker [8].

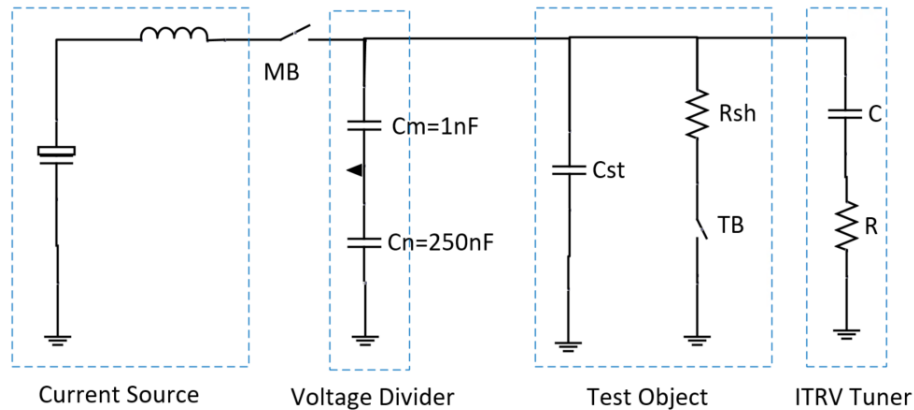


Figure 2.6: Reference test circuit [8].

It is sufficient to apply voltage with the same slope but reduced peak voltage value to evaluate the thermal interrupting limit of the circuit breaker. Further, this method also eliminates the distortion in current wave-shapes near current zero [8].

2.7.2 Ideal experimental setup

There has been several experimental set up circuits built and available [20], [21], [4] and [18]. In contactors dielectric strength and reignition measurement study [4], they use interesting circuit with forward arc quenching process via thyristor and dielectric recovery voltage is applied just by changing the voltage pole of the capacitor and providing reverse path via diode and current limiting resistor. Another experiment uses the quasi-TRV was applied with precise timing by an IGBT connected in parallel to the arcing electrodes. The time $20\ \mu\text{s}$ is a critical point for reignition of a SF_6 -blast arc, and thus the application of the quasi-TRV causes arc re-ignition [18].

In experimental study of [5], [22] and [18] use of micro precision camera is used to capture the picture during process of dielectric behaviour. It gives clarity on understanding the dielectric behaviour. In our experimental set up, there is limitation for use of camera as the arc initiation

to extinction and re strike activity happens in highly pressurised closed nitrogen chamber.

Chapter 3

Experimental Setup

This chapter consists of two sections, the first is simple simulations of expected TRV using MATLAB Simulink. The simulation helps to properly selecting the L and R values to control the current slope before current zero and rate of rise of recovery voltage after current zero. The second part of the chapter is about experimental built up.

3.1 Experimental Simulations

In this section the experimental simulations were carried out using MATLAB simulink software. The expected results of the experimental setup for different values of inductance and resistance are studied. The study results gives better understanding of the behaviour of the circuit parameters under operation.

The circuit is as shown in Figure 3.1 which is simulated for different values of the inductance.

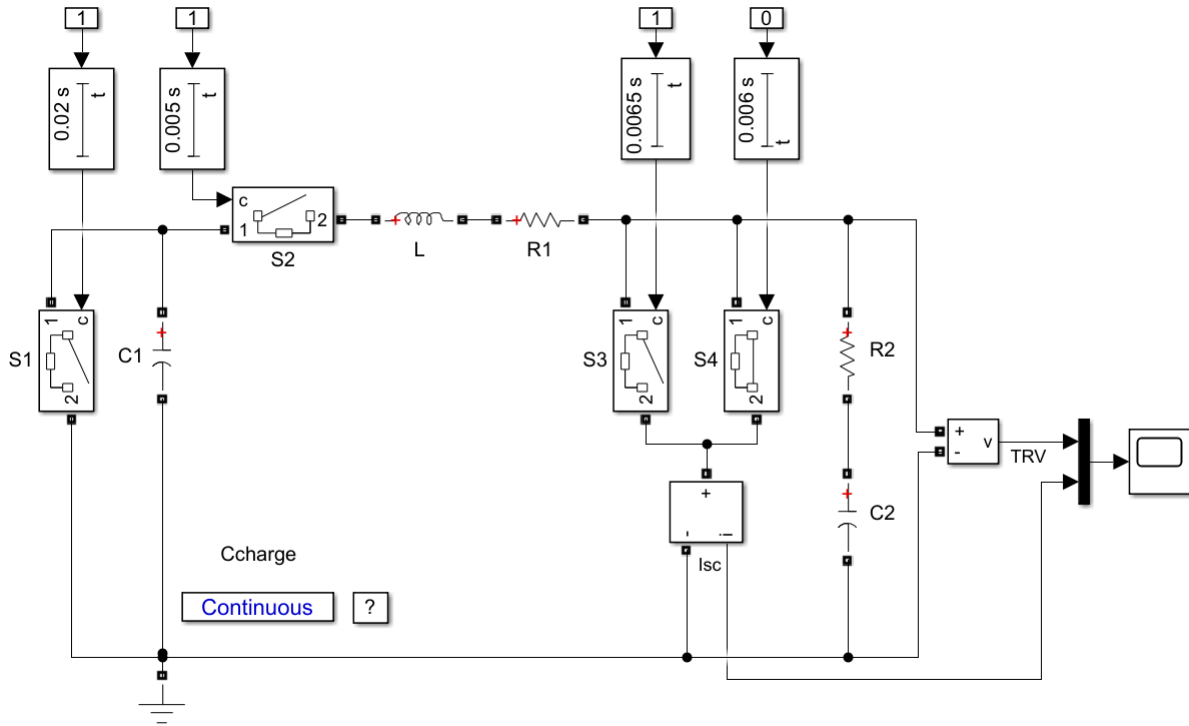


Figure 3.1: Simulation of interruption current (di/dt).

During simulation run, the switch S_1 closes to charge capacitor C_1 to 15 kV, further switch S_2 closes to pass current through inductor L and resistor R_1 . The current will flow through both switch S_4 and also charges capacitor C_2 simultaneously. Switch S_3 is closed after 5 millisecond to demonstrate the transient recovery voltage curve when re-strike happens. In this simulation circuit the simulation is run for period of 0.03 seconds.

3.1.1 Simulation by varying inductance value

In the table 3.1, the circuit parameters along with current slope (di/dt) before current zero are given.

Table 3.1: For various inductance values.

Inductance	I_{peak}	di/dt
[mH]	[A]	[A/ μ s]
12	296.2	1.220
44	155.4	0.332
96	105.4	0.153

The figure 3.2 shows the current interruption and TRV build up for 44mH inductance.

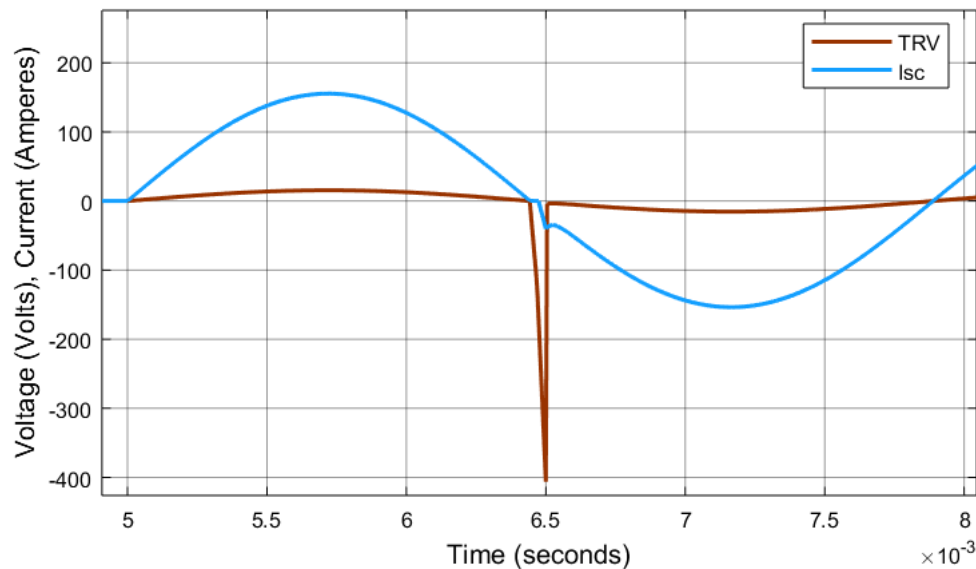


Figure 3.2: Current and voltage waveform for 44 mH inductance.

Variation of the interruption current amplitude is achieved by changing inductance values to 12 mH, 44 mH and 96 mH. It is clear from the table 3.1 that the current amplitude decreases with increase in inductance. It is also shown to make a point that, the current slope (di/dt) value before current zero decrease with increase in inductance value.

The figure 3.3 shows the occurrence of the re strike. Note that the switch S_3 is closed to show how a restrike waveform should look like and slope of TRV curve. The current will remain zero for period of 55 microseconds and again start conducting when TRV recovers.

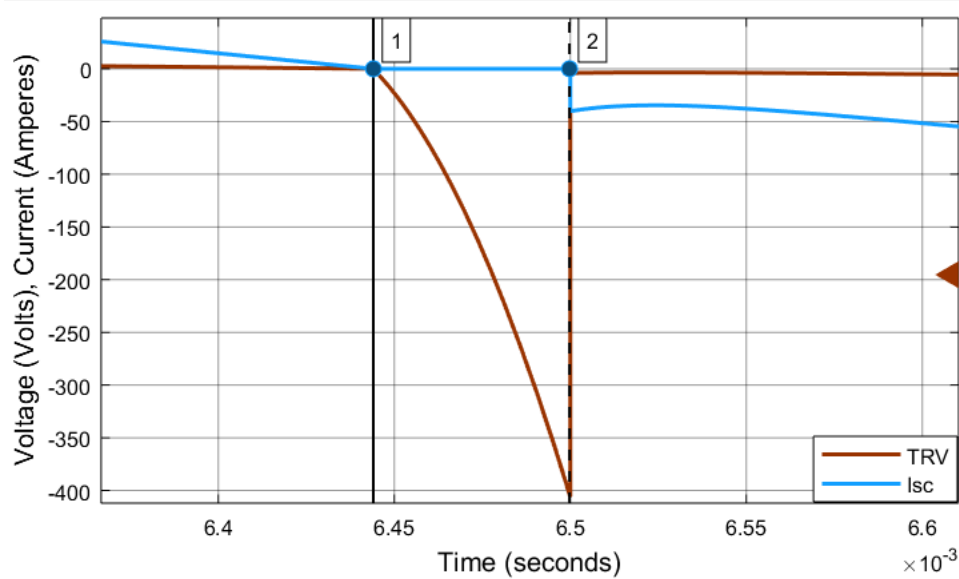


Figure 3.3: Collapse of TRV during closure of switch S3.

3.1.2 Simulation by varying resistance value

In this simulation, the resistor values are changed to control the applied voltage across the electrodes soon after half cycle of the interruption current.

Simulation values for different values of inductance and resistance value are as below :

Table 3.2: For inductance value of 12 mH.

Resistance [ohms]	TRV peak	dv/dt [V/ μ s]	di/dt [A/ μ s]
4.7	-18660	58.682	1.19
47	-15290	63.31	1.188
280	-14290	198.569	1.213

Table 3.3: For inductance value of 44 mH.

Resistance [ohms]	TRV peak	dv/dt [V/ μ s]	di/dt [A/ μ s]
4.7	-19250	31.989	0.333505
47	-16710	31.153	0.333229
280	-14270	59.205	0.333766

Table 3.4: For inductance value of 96 mH.

Resistance	TRV peak	dv/dt	di/dt
[ohms]		[V/ μ s]	[A/ μ s]
4.7	-19470	21.502	0.151773
47	-17490	20.087	0.151808
280	-14500	33.205	0.152485

The values from the tables 3.2, 3.3 and 3.4 show that with the increase in inductance the current slope decreases and vice versa. Higher the di/dt, lesser will be the dielectric recovery time. Lesser the dv/dt (by increased resistance) higher will be the current slope and vice versa. It is also evident that with increase in resistance value TRV slope will also increase gradually. On the other hand, the TRV slope decreases with increase in inductance and vice versa. And also, with increase in resistance value TRV peak will also increase slowly. On the other hand, TRV peak is almost constant for any changes in inductance.

If Capacitor C_2 increases, then lower will be TRV rise and vice versa (This has been observed for couple of values but not made table as we will have fixed capacitance of 2.4 μ F). Note that the simulations are conducted for C_1 , C_2 and R values which are available to use in the lab.

With all of the above simulation studies the below findings can be noticed.

- With the increase in resistance value, the rate of rise of TRV increases and vice versa.
- With the increase in Capacitor C_2 the rate of rise of TRV will be reduced and vice versa.
- As inductance increases, short circuit current decreases and vice versa.
- As inductance increases, current frequency decreases and vice versa.

3.2 Experimental Setup

In this section, the details on experimental set up built in high voltage laboratory is presented. To measure the post arc dielectric recovery performance, an existing test circuit presented in previous work [7] is modified and used in this thesis work. Experimental setup section includes detailed explanation of the test circuit built and its operation along with brief description of the components. Furthermore, procedural steps of conducting the experiment is presented.

The test circuit is as shown in Figure 3.4 which consists of HV source (AC), switch (S_1), resistor-diode unit (R_C - D_C), switch (S_2), inductor (L), resistor (R), capacitors (C_1 and C_2), earthing unit (S_E - R_E) and arcing chamber (pressure vessel).

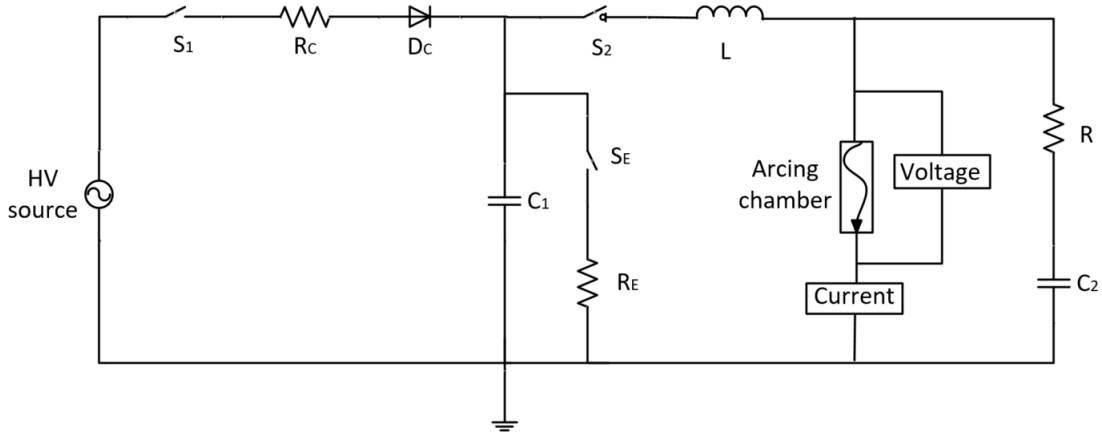


Figure 3.4: Test circuit

Test set up consists of charging and discharging sections. Where charging of the capacitor is done through HV transformer which is controlled through a variac by closing the switch S_1 . The $4.8 \mu\text{F}$ high voltage capacitor C_1 is charged up to 15 kV. Discharging of the stored energy of the capacitor C_1 is done by closing switch S_2 via inductor L . The ignition of the copper wire (sized $25 \mu\text{m}$) inside the pressure vessel takes place due to adiabatic heating which in-turn creates arcing channel. To study the dielectric recovery characteristics, IRRV is controlled as mentioned earlier by changing R . Digital recording of the voltage and current measurements were done via oscilloscope placed in control room. Finally after completion of the test, the circuit is grounded through earthing switch S_E and R_E . The current magnitude is controlled by varying the value of the inductor L and slope of the TRV is controlled by varying the value of the resistor R [7].

This circuit in reality is set in a room built with explosion proof environment. Considering the maximum potential difference that can occur, the circuit is built with standard clearance between adjacent live parts. The lab setup is as shown in the figure 3.5

Ratings of the components are as below :

Resistors	Capacitors	Inductor
$R_C=10 \text{ k}\Omega$, $R_E=250 \text{ k}\Omega$, $R=4.7, 47 \text{ and } 280 \Omega$	$C_1=4.8 \mu\text{F}$ $C_2=2.4 \mu\text{F}$	$L=12, 44 \text{ and } 96 \text{ mH}$

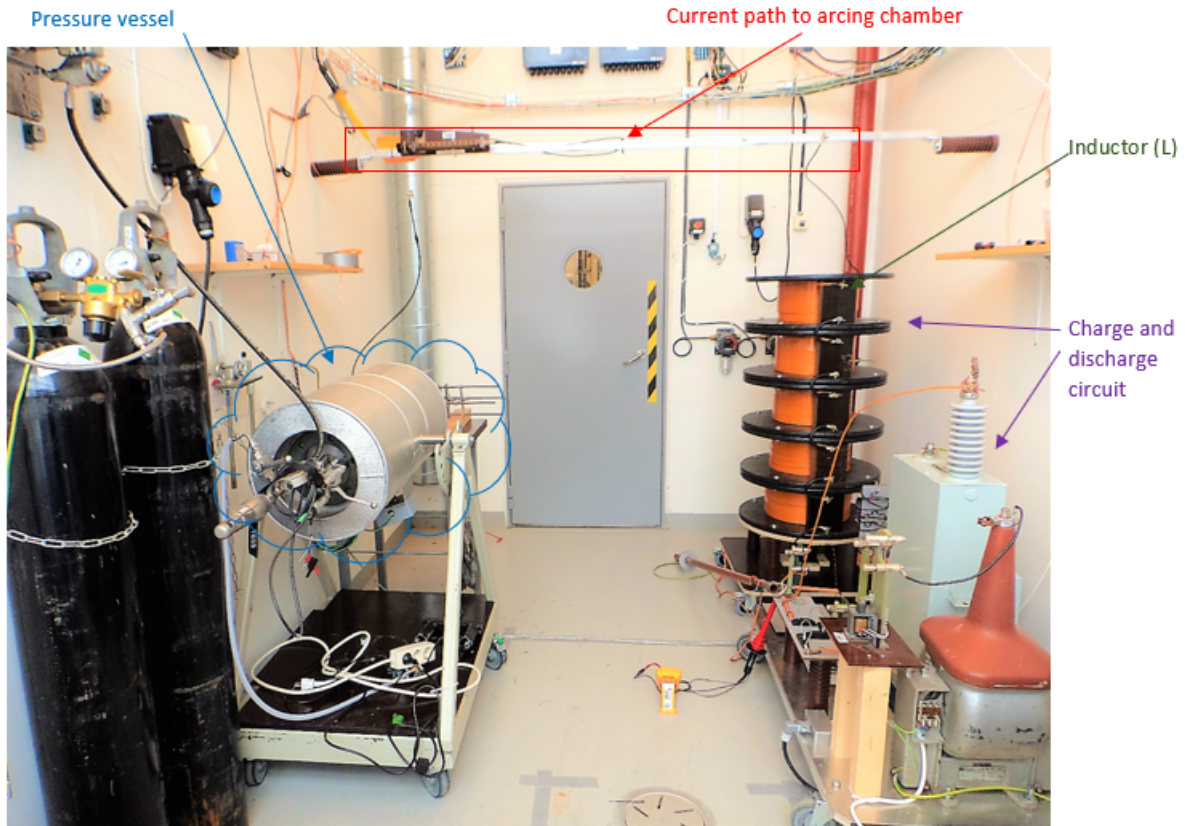


Figure 3.5: Complete circuit set up in laboratory.

Each component on the setup table are as shown in figure 3.6 as per nomenclature used in circuit.

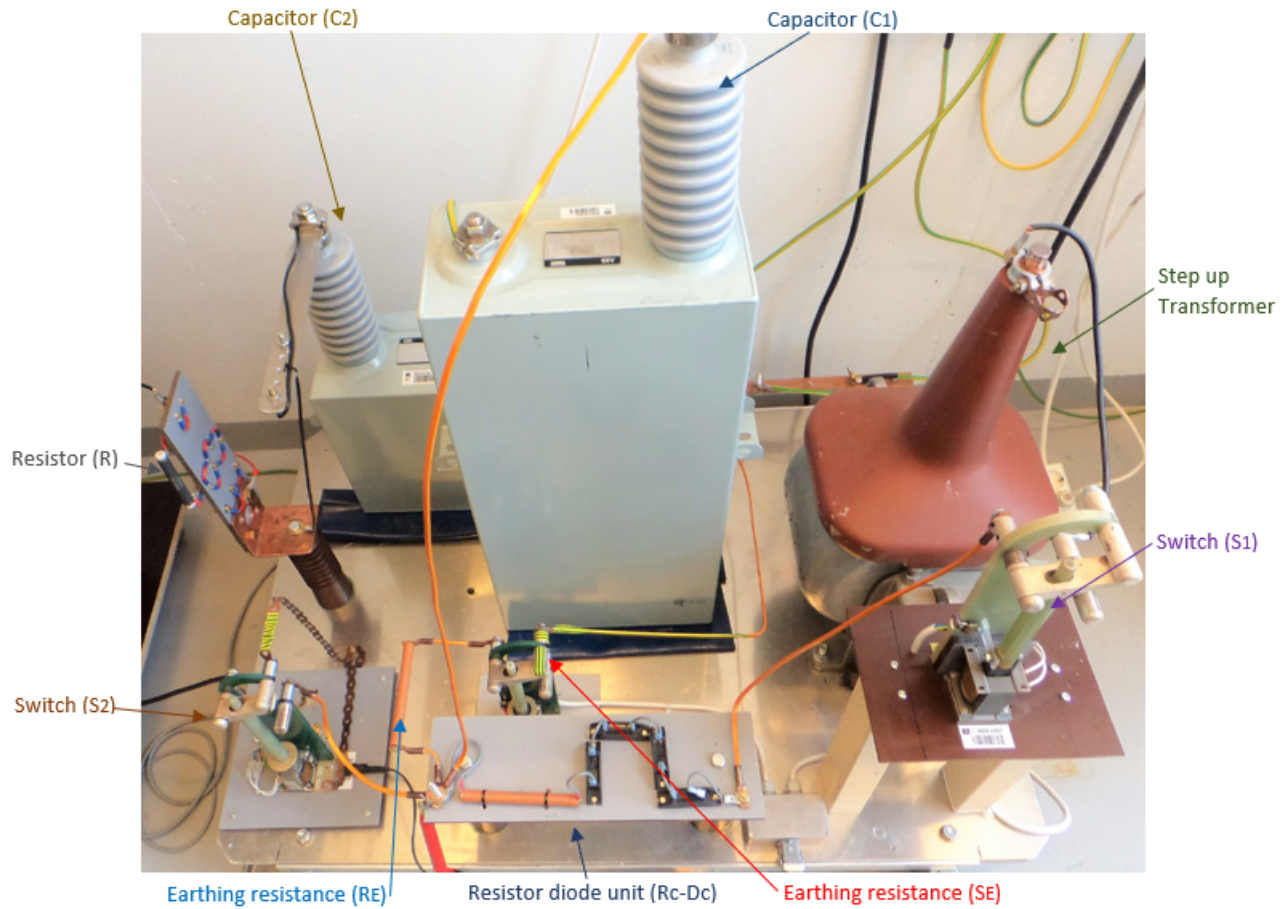
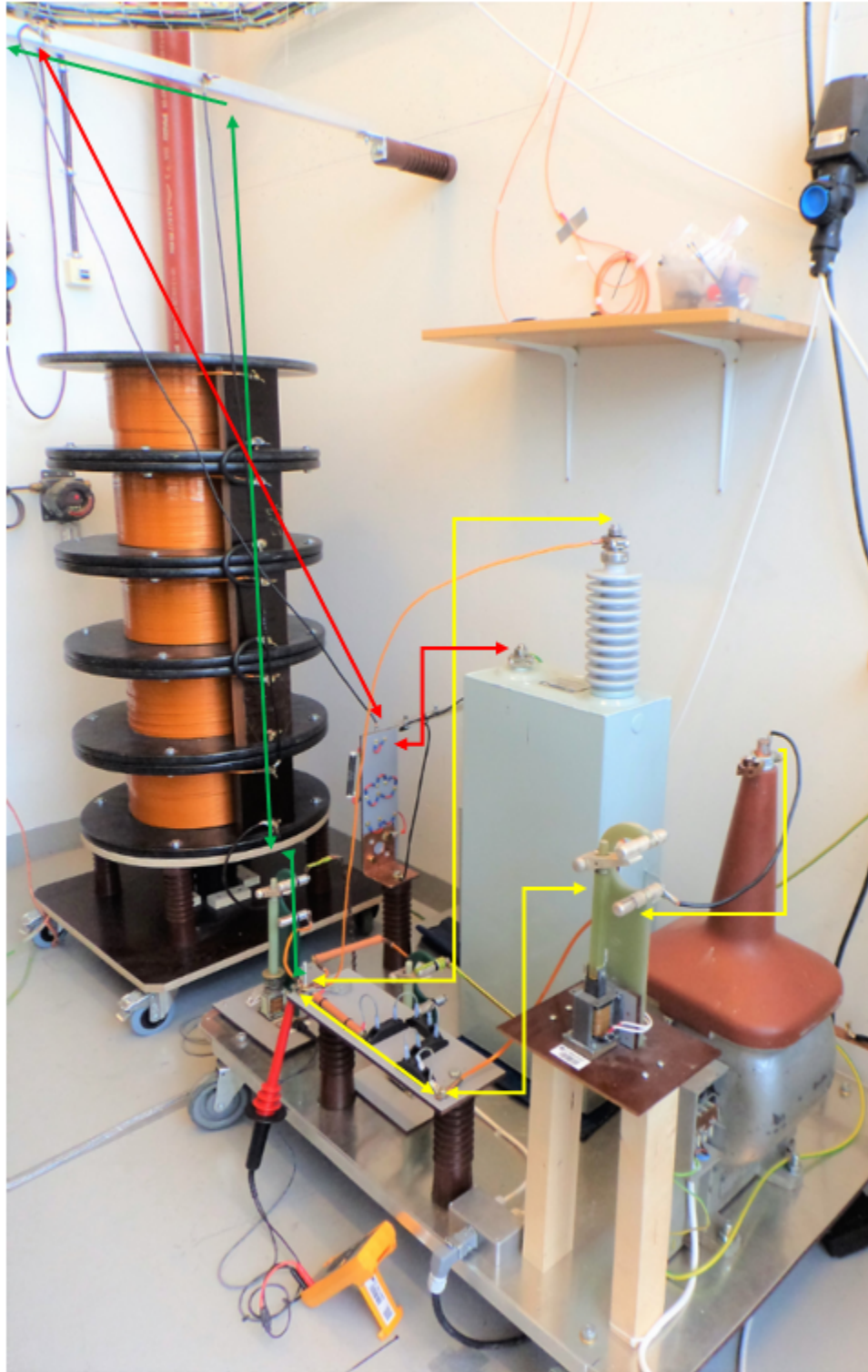


Figure 3.6: Circuit components mounted on table.

The test set up at lab which have three circuit path is shown in figure 3.7 along with marking of each path in different colour.



- Ac Power -> Switch (S1) -> Resistor Diode (Rc-Dc) -> Capacitor (C1)
- Switch (S2) -> Inductor (L) -> Pressure vessel (Arcing chamber)
- Capacitor (C2) -> Resistor (R) [IIRV controlling part]

Figure 3.7: Circuit paths in laboratory setup.

Pressure vessel schematic is shown in Figure 3.8 which consists of 24 kV miniature HV cable which is fed through the flange of the pressure tank firmly in support with several insulating supports. Two copper-tungsten (CuW) electrodes separated by fixed distance of 30 millimetre for all the experiments. Ignition wire is fixed between these CuW electrodes. The supporting metal structure along with flange acts as return path of the current. Voltage and current measurements are carried out through HV probe and current shunt respectively. These values are communicated to control room via fiber optics and stored in a digital oscilloscope [7].

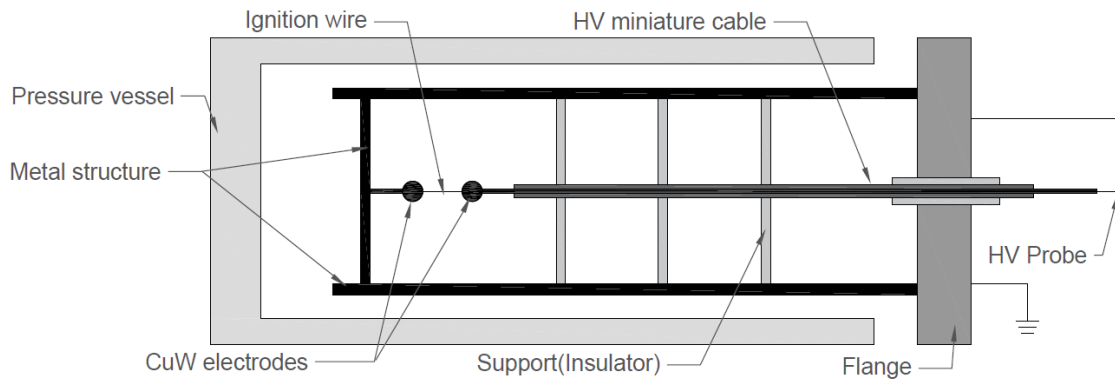


Figure 3.8: Pressure vessel schematic [7].

As it can be seen from the schematic it consists of two parts, first being pressure vessel and second being the complete supporting metal structure consisting of electrodes and ignition wire.

Pressure vessel used for experiment is as shown in figure 3.9 and 3.10.

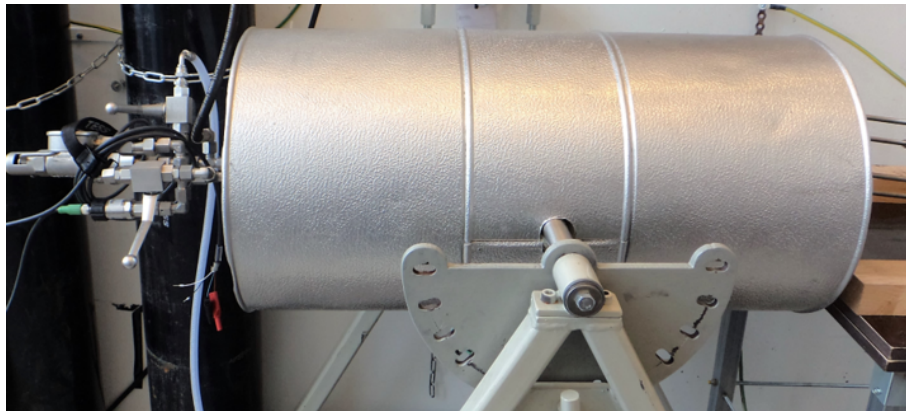


Figure 3.9: Side view of Pressure vessel.



Figure 3.10: Inside chamber of pressure vessel.

Firmly mounted copper tungsten electrodes for ignition wire connection is as shown in figure 3.11.

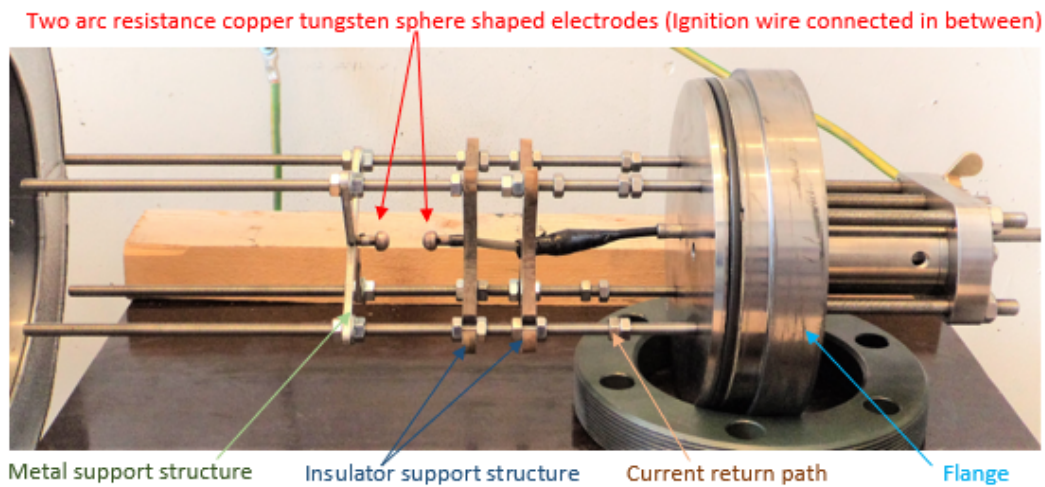


Figure 3.11: Flange housing.

Measurement probes and transmitters along with optical fiber data transmission inside lab set up room is as shown in figure 3.12.

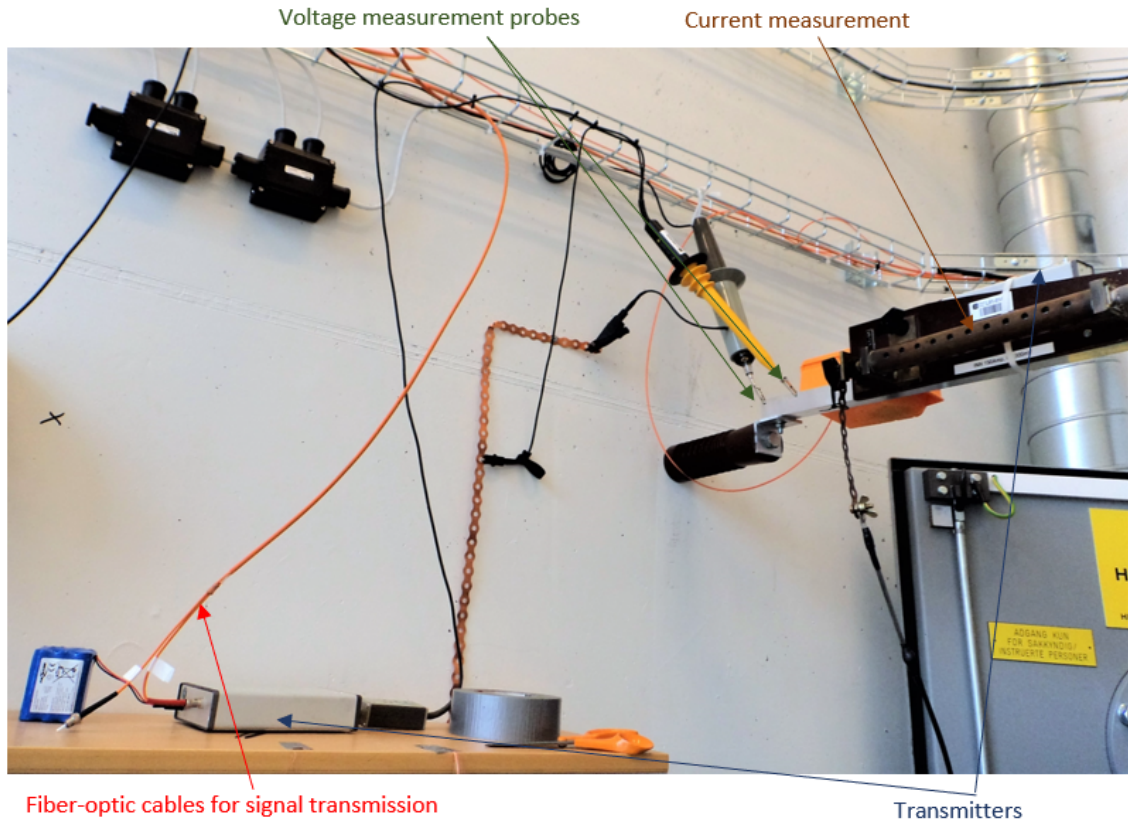


Figure 3.12: Measurement probes setup.

Experimental set up room is operated with high voltage (15 kV) charging and discharging. For safety of personal, the circuit control operations are done from separate control room. Charging/discharging operations are done through remote switches. Gas filling and emptying the pressure vessel is done also remotely. Gas filling pressure is measured via digital display kept in complete control room set up as shown in figure 3.13.

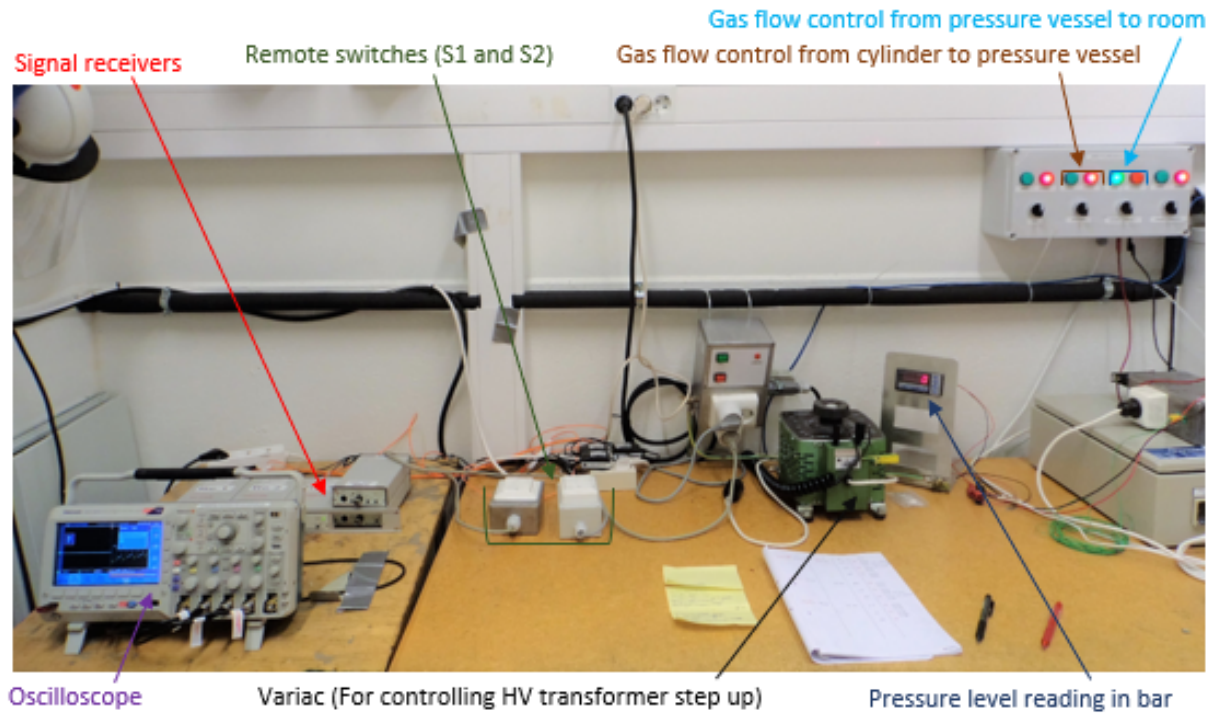


Figure 3.13: Control room setup.

Measurements and waveforms are read from oscilloscope via signal receivers located in control room. Two channels are used for voltage measurement while one channel is used for current measurement as shown in figure 3.14. As both the arc voltage and the TRV are of interest, two voltage probes were used.

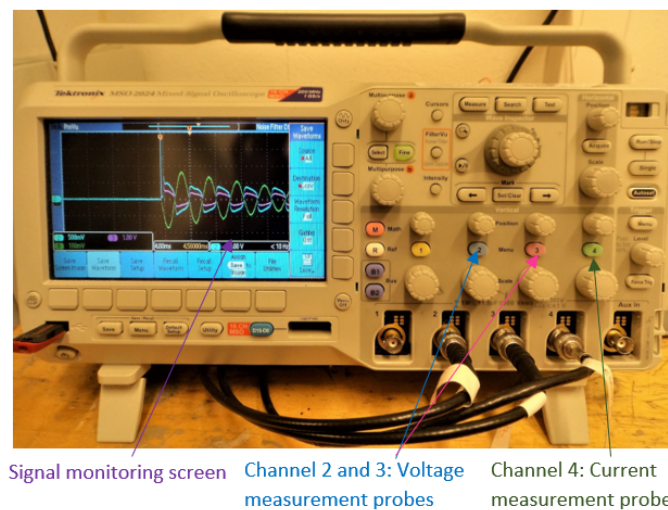


Figure 3.14: Oscilloscope.

3.2.1 Experimental procedures

Experiment is conducted step wise starting from charging of the circuit to earthing of the circuit is as below :

Preparation: Pressure vessel is flushed with industrial grade nitrogen (quality of 99% nitrogen) for every experiment conducted. After experiment the over-pressure is released and moving flange part is removed to connect new ignition wire for next experiment.

- 1) HV source connected to power supply.
- 2) Switch S_1 is closed remotely.
- 3) Capacitor C_1 is charged up to 15 kV through resistor-diode R_C - D_C unit.
- 4) Switch S_1 is opened.
- 5) Knife switch S_2 is closed remotely and Capacitor C_1 is discharged through inductor L and across arcing chamber.
- 6) After current zero the voltage of capacitor C_2 along with resistor R appear across the arcing chamber.
- 7) Dielectric re-strikes voltage and current values will be recorded through digital oscilloscope.
- 8) The test circuit is de-energised by closing earthing switch S_E via earthing resistor R_E once the test is over.
- 9) Experiment repeated from step 2 to 8 for different filling pressure of N_2 and by varying inductance L and resistance R values.

The test cases and conditions are as shown in the table 3.5.

Table 3.5: Test cases and values.

Charging voltage	Capacitor (C_1)	Inductance (L)	Current Amplitude	Frequency
[kV]	[μ F]	[mH]	[A]	[Hz]
15	4.8	96	150	236
15	4.8	44	150	350
15	4.8	12	150	670

The experiments are conducted for three different pressure of 1 bar, 20 bar and 40 bar. The interruption current amplitude (di/dt) is varied by changing the inductance(L) value for three different values of 12, 44 and 96 millihenry. The time period of TRV (dv/dt) is varied by changing the resistance (R) values to three values of 4.7, 47 and 280 ohms.

At least three experiments are conducted for any tested combination of pressure, inductance and resistance. The average of these values are analysed and discussed in experimental results chapter. Total of 81 [3(pressure)x3(inductance)x3(resistance)x3(tests)] tests were conducted in this thesis.

3.2.2 Technical details of measurement devices

Optical fiber cable is used for signal transformation from measuring probes located in experiment room to the oscilloscope located in control room. Firstly, because of its immunity to electromagnetic interference present in experiment area. Secondly, as it do not conduct electricity, preventing problems with ground loops. Finally due to its broad bandwidth conduction capability.

P6015A-1000X High Voltage Probe

The P6015A is a ground-referenced 100 mega-ohm, 3.0 pF high voltage probe with 1000X attenuation. It adds high-voltage measurement capability to oscilloscopes and other measurement devices having an input resistance of 1 mega-ohm and an input capacitance of 7 pF to 49 pF [23]



Figure 3.15: P6015A-1000X High Voltage Probe [23].

The maximum input voltage level is 1.5 to 20 kV DC+AC peak. Voltage ration is 1000:1 with DC attenuation of $\pm 3\%$ excluding oscilloscope error and at test conditions oscilloscope input

resistance must be 1 mega-ohm with error margin of $\pm 2\%$. Temperature coefficient of DC attenuation being $\pm 0.006\%$ per degree Celsius and voltage coefficient of DC attenuation $\pm 0.018\%$ per kV. Test oscilloscope bandwidth must be ≥ 100 MHz [23].

HVP 15HF High Voltage Probe

The HVP 15 HF is high voltage oscilloscope probe. The maximum input voltage level is 0 to 15 kV DC [24].



Figure 3.16: HVP 15HF High Voltage Probe [24].

Voltage ratio is 1000:1 with DC attenuation of $\pm 1\%$ until 10 kV and $\pm 2\%$ from 10 to 15 kV. excluding oscilloscope error and at test conditions oscilloscope input resistance must be 1 mega-ohm with error margin of $\pm 0.5\%$. Test oscilloscope bandwidth is DC~ 50 MHz (-3dB) [24].

LTX-5510R signal transmitter

The LTX-5510R Electrical to Optical and Optical to Electrical Converter system comprise a convenient product that is intended to transmit analog and digital information to a remote location via fiber optic cable [25].

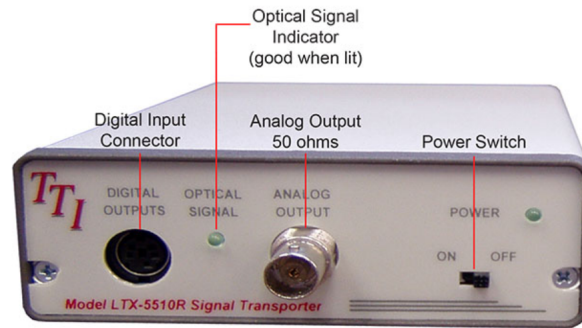


Figure 3.17: LTX-5510R signal transmitter [25].

These systems transmit an analog signal plus four digital input channels simultaneously. The input analog signal may range in frequency from DC to 12.5 MHz (-3 dB point). The digital signals may switch at up to 12 MHz and are independent. The analog input may be terminated at 1 mega-ohm or 50 ohms depending on the front panel switch. The output impedance is always 50 ohms. Analog signals may range from -5 to +5 volts. The output signal will have a one to-one correspondence, i.e. a gain of +1. When the front panel selector switch is set to +/- 1V the gain is +5, i.e. a 1 volt input signal will result in a five volt output signal. The data transfer accuracy is $\pm 0.1\%$ Full Scale, ± 20 mV offset [25].

MSO 2024 Mixed Signal Oscilloscope

Oscilloscopes are used to observe the change of an electrical signal over time, such that voltage and time describe a shape which is continuously graphed against a calibrated scale. The observed waveform can be analysed for such properties as amplitude, frequency, rise time, time interval, distortion and others.

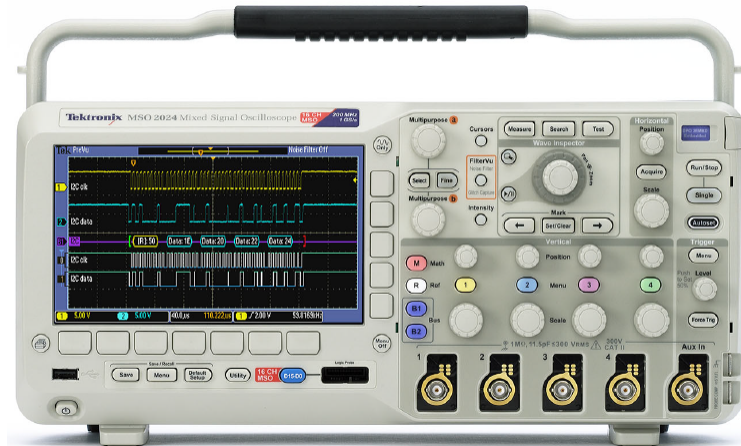


Figure 3.18: MSO 2024 Mixed Signal Oscilloscope [26].

This oscilloscope has 4 input channels in which we have used channel 2 and 3 for voltage measurement and channel 4 for current. The analog bandwidth of 200 Hz and the DC gain accuracy with offset set to zero offset $\pm 3\%$ for 10 mV/div to 5 V/div, $\pm 4\%$ for 2 mV/div to 5 mV/div. The waveform capture rate of up to 5000 wfm per second. It also supports USB 2.0 high speed output port. The recorded wave forms are saved in .CSV format to external pen drive for further evaluation [26].

Chapter 4

Experimental Results

In this master thesis study the characteristics of free burning arc after current zero in nitrogen chamber for different filling pressures are explored. As for the previous current interruption studies [20], [21], [4] and [18], the supercritical fluids have shown combined benefits of both liquid and gaseous state. To explore further the characteristics of free burning arc at pressure values of 1, 20 and 40 bar are conducted. This chapter includes the experimental results based on the methodology adopted from chapter 2 and experimental setup described in chapter 4.

4.1 Experimental data

The procedure of experiment conduction until data are recorded in .CSV files is already been discussed in chapter 3. The results obtained for atmospheric pressure (1 bar), 20 bar and 40 bar are tabulated in respective subsection.

4.2 Data processing

Measured data were imported to MAT-lab and data is processed. Due to presence of electromagnetic interference with measured values and error margins, the waveform recorded has high-frequency noise in the raw measurement.

The measured value for one of the test criterion having the test set up connected to 44 mH inductance and 47 Ω resistance conducted at atmospheric pressure (1bar) is as shown in figure 4.1.

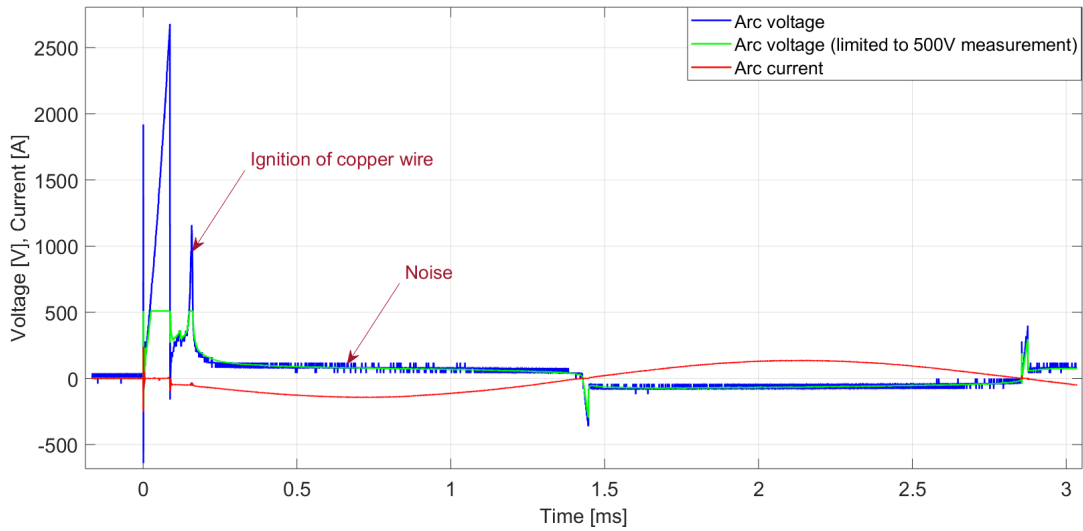


Figure 4.1: Measured arc voltage and current at atmospheric (1bar) pressures and 30-mm electrode gap.

This data is further filtered to get smoothed curve. The 'loess' method is used for smoothing (filtering) and to remove the inherent high-frequency noise present in the measurement. where in the 'loess' method works on principle of local regression using weighted linear least squares and a 2nd degree polynomial model [27]. The smoother curve for the test criterion having the test set up connected with 44 mH inductance and 47 ohms resistance conducted at atmospheric pressure (1bar) is as shown in figure 4.2.

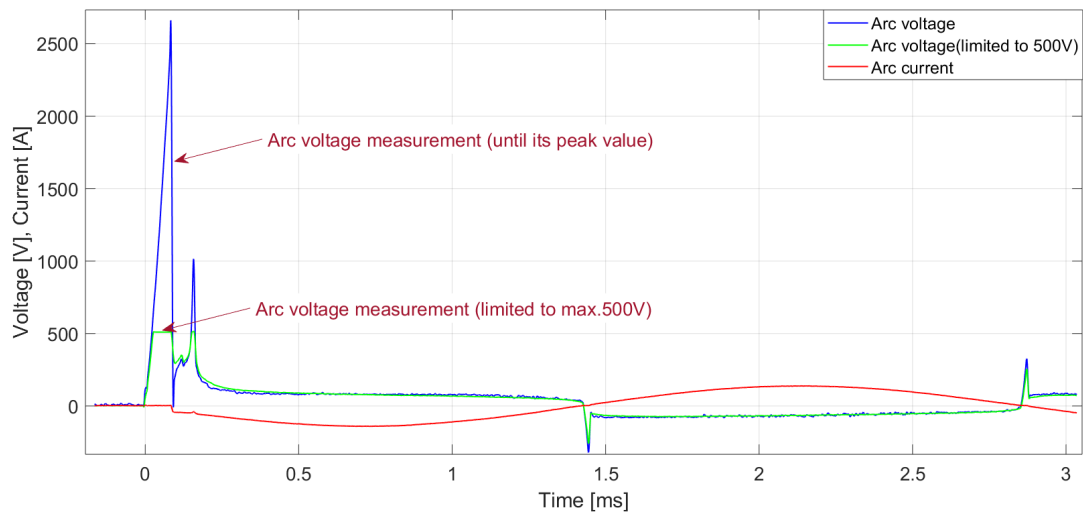


Figure 4.2: Measured arc voltage and current with filter at atmospheric (1bar) pressures and 30 mm electrode gap.

Closer look of the wave forms near TRV is as shown in figure 4.3, 4.4.

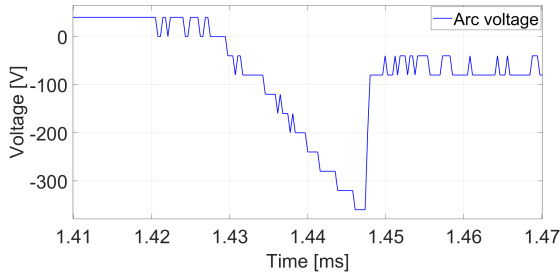


Figure 4.3: At TRV without filter.

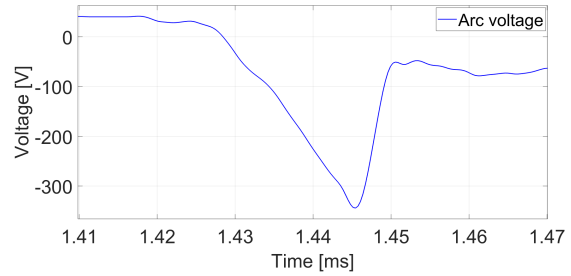


Figure 4.4: At TRV with filter.

Further the data points before current zero (for current slope) and after current zero until current again starts to rise (for current zero time period) for restrike are noted. For TRV curve two data points (for TRV slope) are marked along with the peak point of TRV curve. An example of the data points from the filtered waveform for one of the criterion is shown in the figure 4.5.

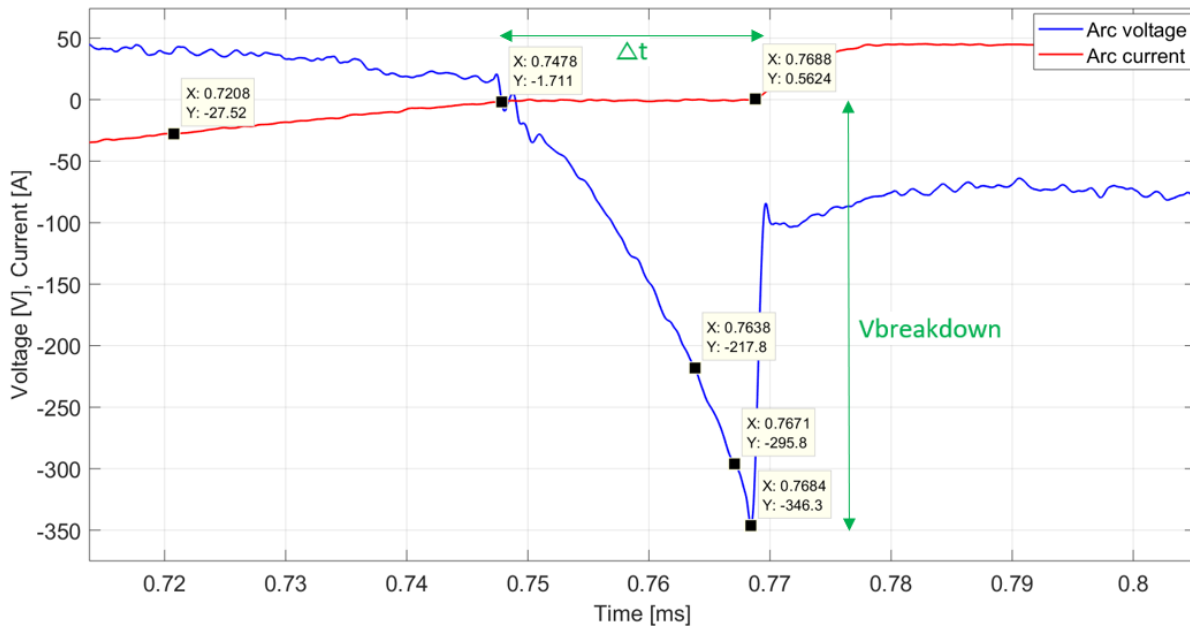


Figure 4.5: Typical data points for slope and current zero time period calculation.

Current and TRV slopes are calculated by using formula

$$Slope = \frac{y_2 - y_1}{x_2 - x_1}$$

The values of extracted data from each of the experimental readings are listed as shown in respective criterion subsections.

Initial voltage rise: The curve shown is for the test set up connected with 12 mH inductance and 4.7 Ω resistance conducted at atmospheric pressure (1bar). Only two probe measurement takes for this test (current and voltage).

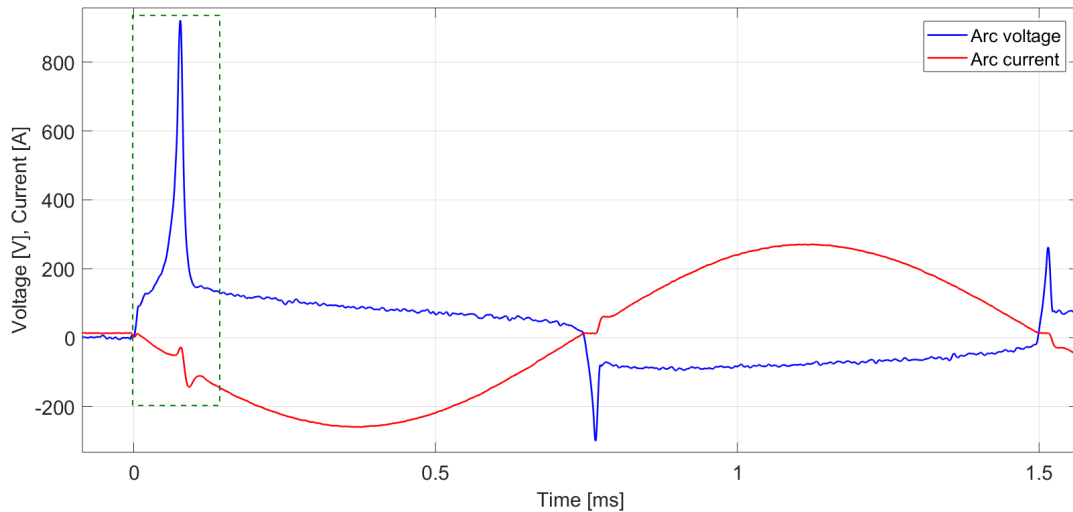


Figure 4.6: Measured arc voltage and current with filtered wave forms at atmospheric (1bar) pressures and 30 mm electrode gap.

In the figure 4.6, After energising the circuit when the switch S_2 is closed, a sharp increase in voltage is observed. Due to joule heating, the voltage drop across the copper wire increases until peak value of the voltage just before 0.1 ms. This peak value of the voltage occurs because of evaporation of the copper wire connected between electrodes and formation of arc channel between them. No sooner the arc is established between the electrodes, the initially risen peak voltage drops quickly to stable value. As the current continues to flow, the arc voltage will continue to decrease slowly with time until current zero [7].

Further it can be observed closely for delay in re-strike (Δt) period which is 18.3 μs . The peak value of the voltage at re-strike is found to be approximately 346.9 volts. The figure 4.7 clearly shows the momentary interruption of current and its re-ignition.

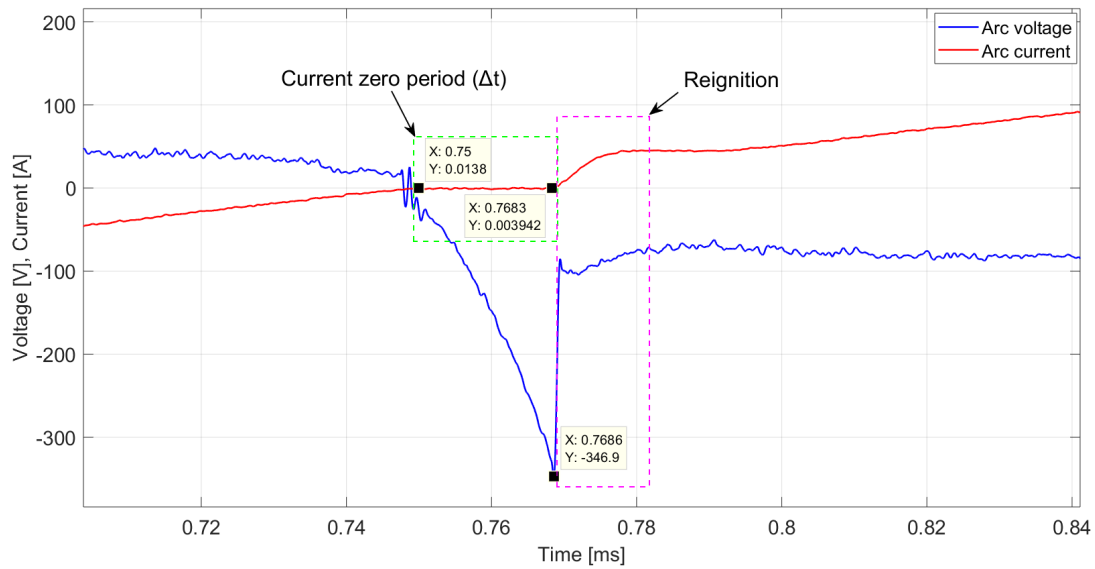


Figure 4.7: Current zero period and re ignition occurrence.

4.3 Case studies

The information extracted from the experimental results obtained from experiments conducted are plotted for in their respective subsections.

4.3.1 For atmospheric(1 bar) pressure

The plots from experimental results for 1 bar pressure are as in figures 4.8, 4.9, 4.10 and 4.11.

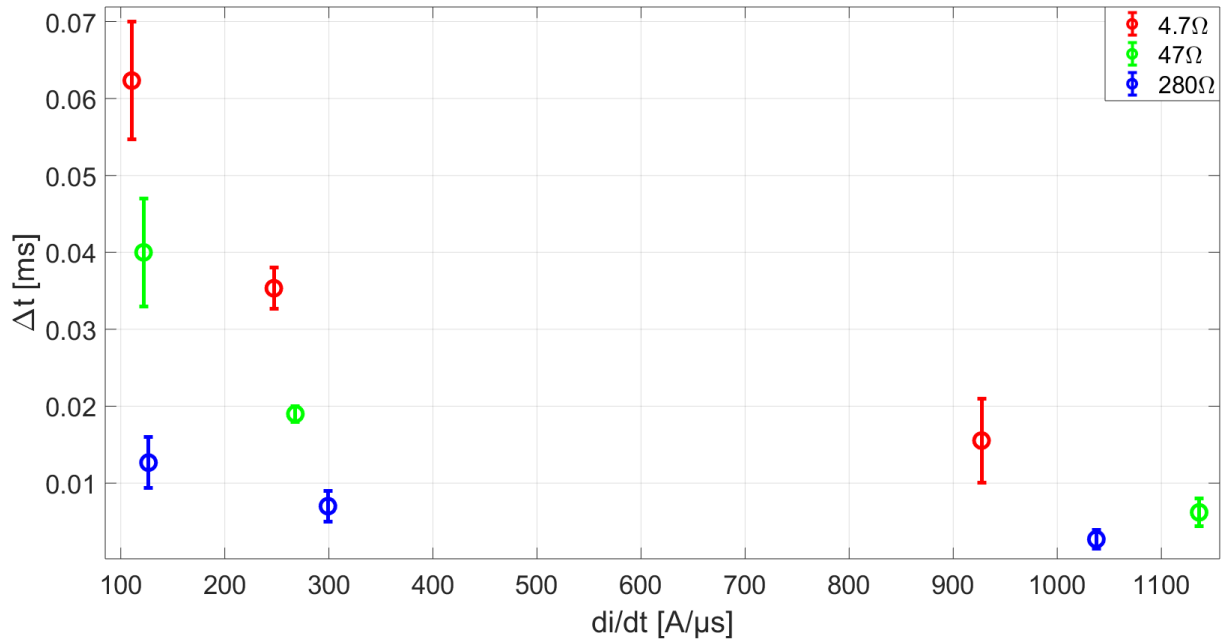


Figure 4.8: Delay in restriking (Δt) versus rate of change of current (di/dt) just before current zero at 1 bar pressure.

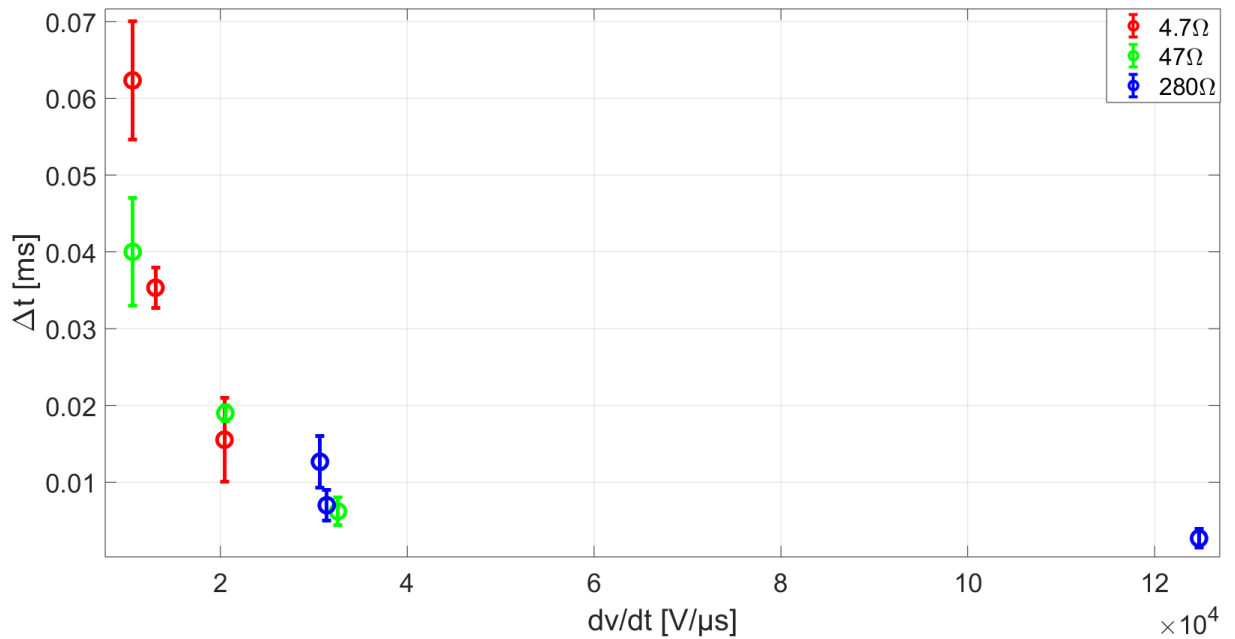


Figure 4.9: Delay in restriking (Δt) versus rate of change of TRV (dv/dt) after current zero at 1 bar pressure.

Figure 4.8 shows that for 96 mH inductance the di/dt remains slightly around at 125 A/ms but Δt

varies largely between 0.012 to 0.065 milliseconds for different values of resistance. Higher the R, lower the Δt . This is expected as high R will impose steep IRRV and the restrike occurs earlier. This can be shown clearly from above figures 4.8 and 4.9. Further as inductance value decreases to 44 mH, the di/dt differs marginally between 225 to 300 A/ms and Δt decreases to range between 0.008 to 0.038 milliseconds. For lowest inductance value of 12 mH, di/dt increases in large range from 950 to 1150 A/ms but Δt varies marginally between 0.002 to 0.015 milliseconds.

Overall, the time delay to restrike (Δt) is highest for 4.7 Ω resistance values followed by 47 Ω and 280 Ω respectively. A common trend of decreased Δt and high increase di/dt is observed for increased resistance and decreased inductance.

In the figure 4.9, it can be shown that high dv/dt results in low Δt . The Δt is highest for 4.7 Ω resistance values followed by 47 Ω and 280 Ω respectively. The dv/dt range 4.7 Ω is found to be in varying slightly. For 47 Ω its range increase marginally and for 280 Ω , its range is found to be largest. Here a common trend of decreased Δt , with increase dv/dt is observed.

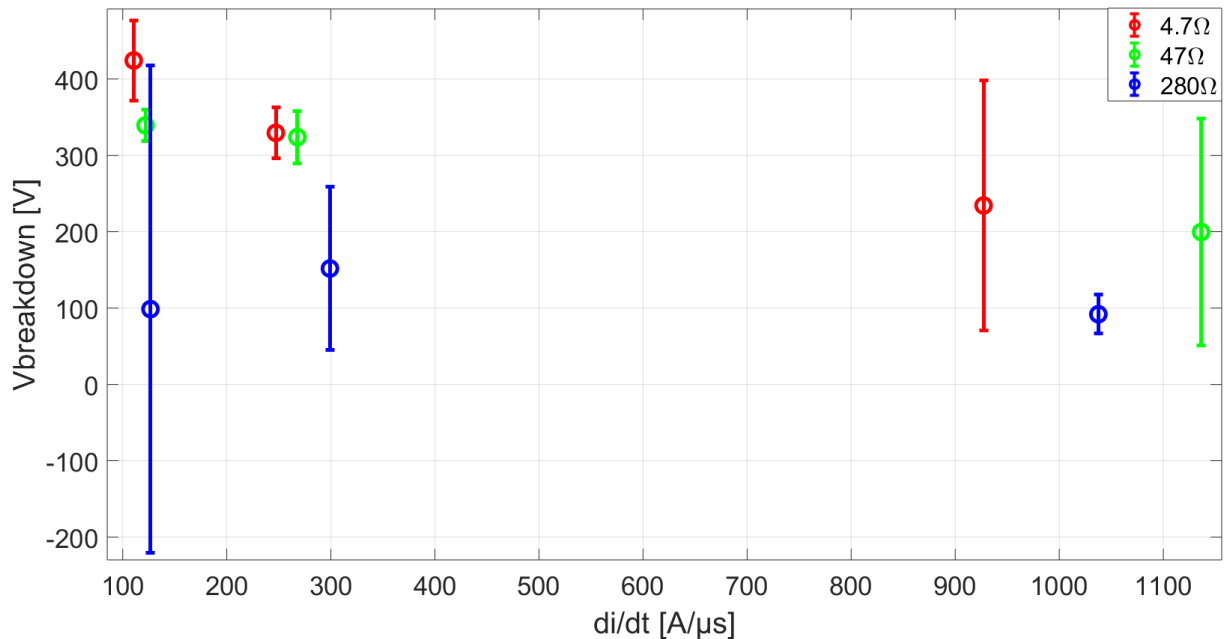


Figure 4.10: Breakdown voltage versus rate of change of current (di/dt) just before current zero at 1 bar pressure.

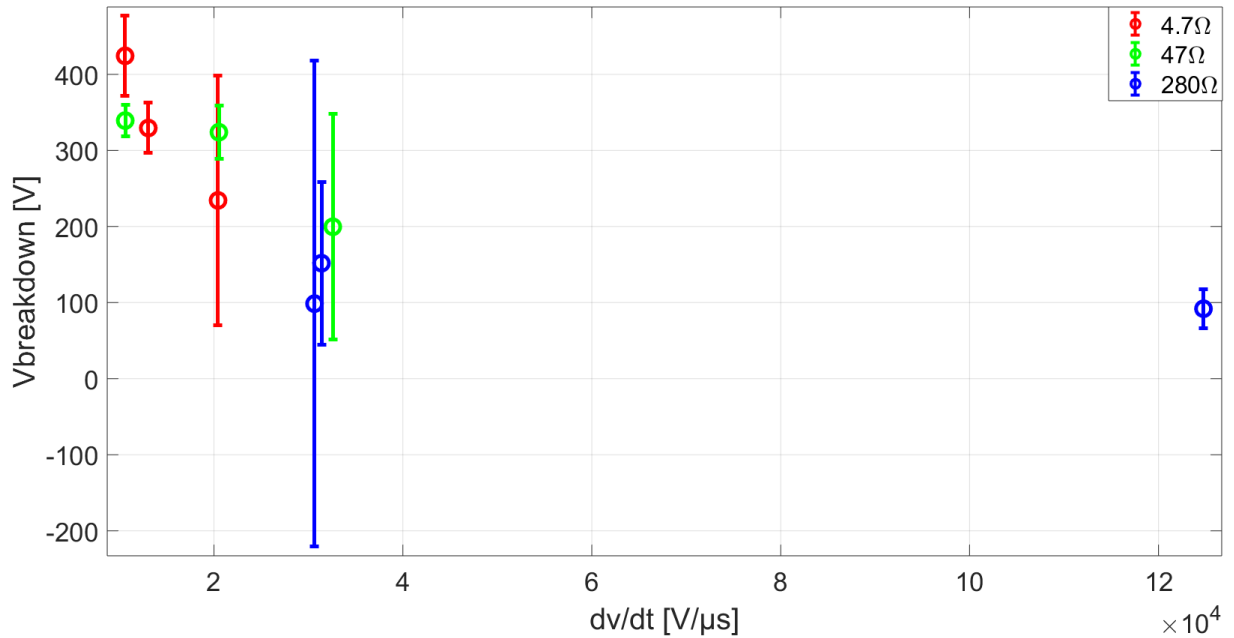


Figure 4.11: Breakdown voltage versus rate of change of TRV (dv/dt) after current zero at 1 bar pressure.

Figure 4.10 shows that for 96 mH inductance the di/dt remains slightly around at 125 A/ms but breakdown voltage varies largely in range of 300 volts for different values of resistance. Further as inductance value decreases to 44 mH, the di/dt value found to have increased value between 250 to 300 A/ms and breakdown voltage range decreases to 175 volts. For lowest inductance value of 12 mH, di/dt increases in large range from 950 to 1150 A/ms but breakdown voltage range again increases to 225 volts.

Overall, the breakdown voltage is found highest for 4.7 Ω resistance values followed by 47 Ω and 280 Ω respectively. The di/dt value keep increasing for increased resistance and decreased inductance.

Figure 4.11 shows that for 96 mH inductance the dv/dt remains slightly around at 12500 to 31000 V/ms but breakdown voltage varies largely in range of 400 volts for different values of resistance. Further as inductance value decreases to 44 mH, the dv/dt value found to have slightly less value between 15000 to 32500 V/ms and breakdown voltage range decreases to 225 volts. For lowest inductance value of 12 mH, dv/dt increases in large range from 20000 to 125000 V/ms but breakdown voltage range again increases to 225 volts.

Overall, the breakdown voltage is found highest for 4.7 Ω resistance values followed by 47 Ω and

280 Ω respectively. The dv/dt value keep increasing for increased resistance and decreased inductance.

4.3.2 For 20 bar pressure

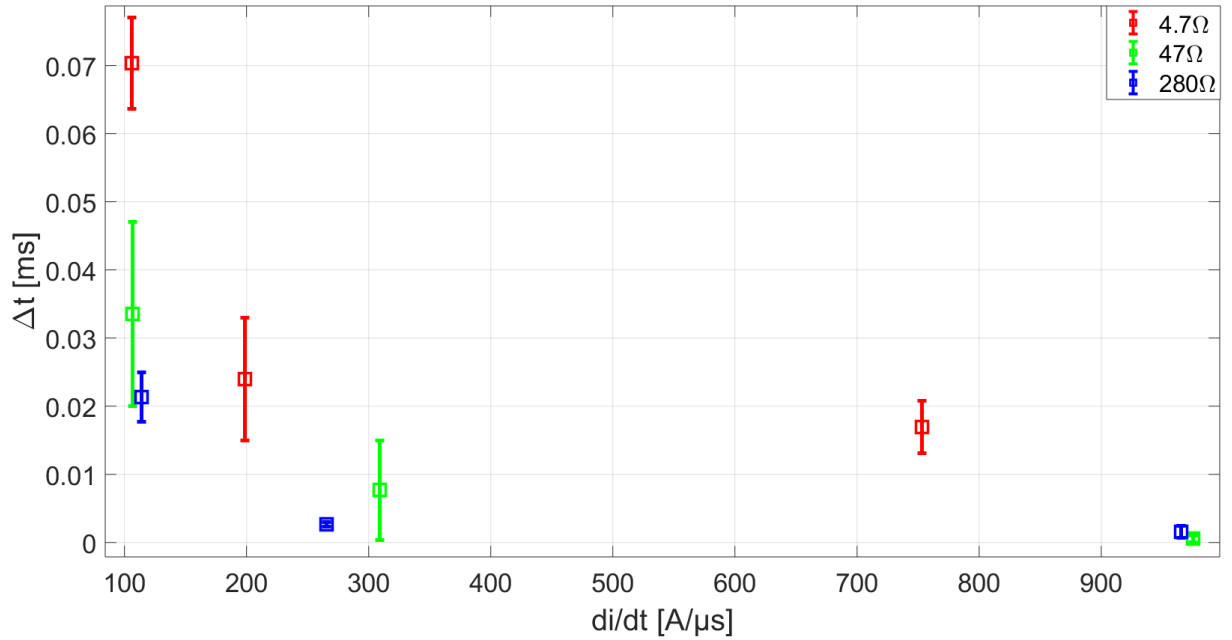


Figure 4.12: Delay in restriking (Δt) versus rate of change of current (di/dt) just before current zero at 20 bar pressure.

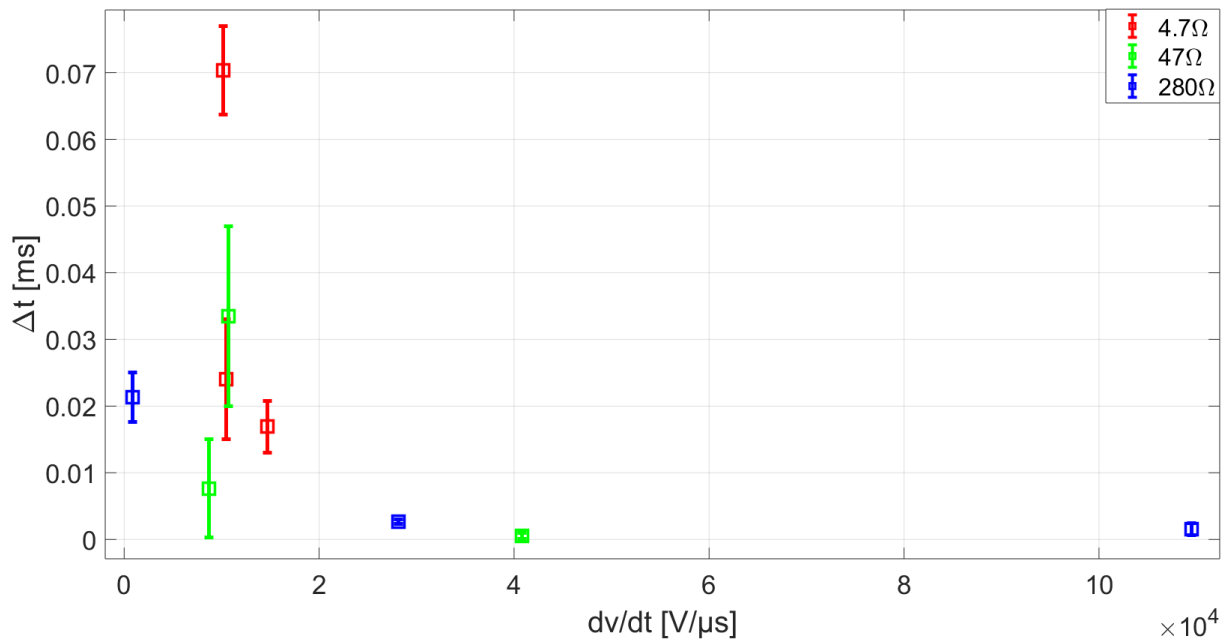


Figure 4.13: Delay in restriking (Δt) versus rate of change of TRV (dv/dt) after current zero at 20 bar pressure.

Figure 4.12 shows that for 96 mH inductance the di/dt remains slightly around at 100 A/ms but Δt varies largely between 0.02 to 0.07 milliseconds for different values of resistance. Higher the R , lower the Δt . This is expected as high R will impose steep IRRV and the restriking occurs earlier. This can be shown clearly from above figures 4.12 and 4.13. Further as inductance value decreases to 44 mH, the di/dt differs marginally between 200 to 310 A/ms and Δt decreases to range between 0.001 to 0.025 milliseconds. For lowest inductance value of 12 mH, di/dt increases in large range from 750 to 980 A/ms but Δt varies marginally between 0.001 to 0.016 milliseconds.

Overall, the time delay to restriking (Δt) is highest for 4.7 Ω resistance values followed by 47 Ω and 280 Ω respectively. A common trend of decreased Δt and high increase di/dt is observed for increased resistance and decreased inductance.

In the figure 4.9, it can be shown that high dv/dt results in low Δt . The Δt is highest for 4.7 Ω resistance values followed by 47 Ω and 280 Ω respectively. The dv/dt range 4.7 Ω is found to be in varying slightly. For 47 Ω it is found to be increasing considerably. For 280 Ω , its range is found to be largest. Here a common trend of decreased Δt , with increase dv/dt is observed.

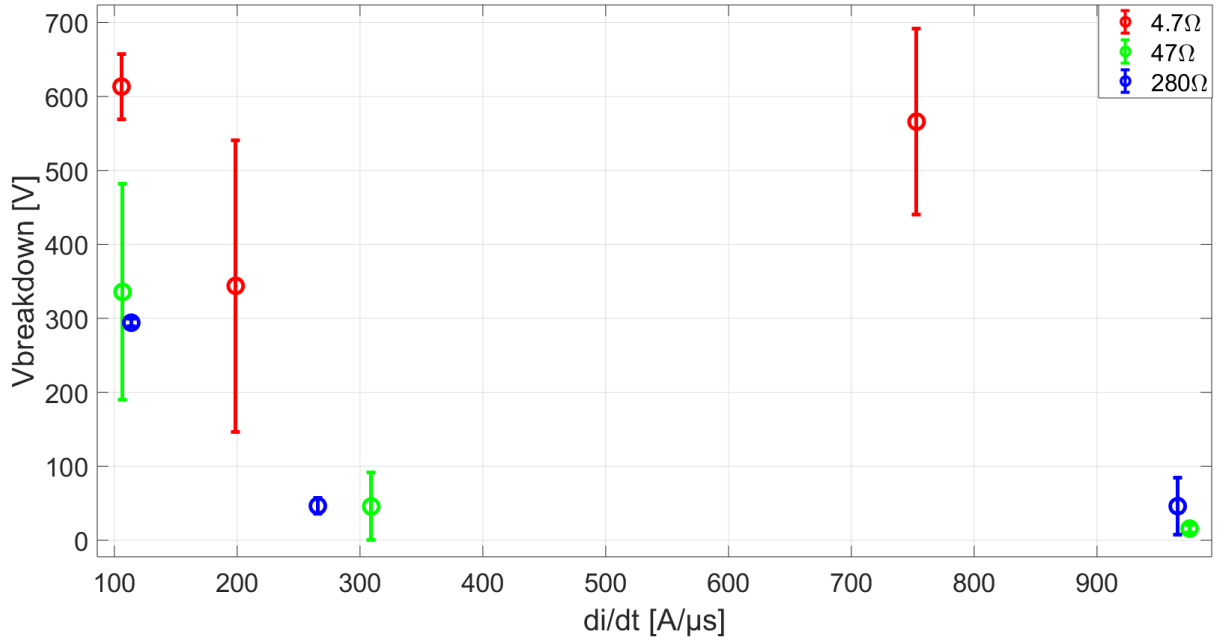


Figure 4.14: Breakdown voltage versus rate of change of current (di/dt) just before current zero at 20 bar pressure.

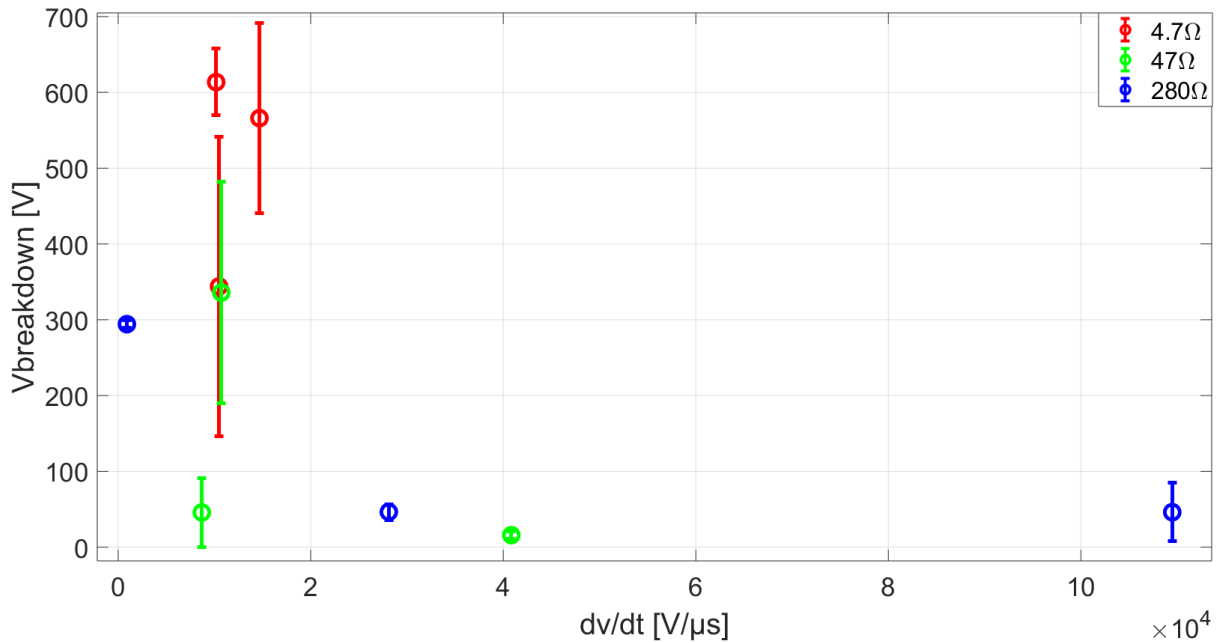


Figure 4.15: Breakdown voltage versus rate of change of TRV (dv/dt) after current zero at 20 bar pressure.

Figure 4.14 shows that for 96 mH inductance the di/dt remains slightly around at 110 A/ms but

breakdown voltage varies largely in range of 300 volts for different values of resistance. Further as inductance value decreases to 44 mH, the di/dt value found to have increased value between 200 to 310 A/ms and breakdown voltage range remains same to 300 volts. For lowest inductance value of 12 mH, di/dt increases in large range from 750 to 975 A/ms but breakdown voltage range being largest value of 575 volts.

Overall, the breakdown voltage is found highest for 4.7 Ω resistance values followed by 47 Ω and 280 Ω respectively. The di/dt value keep increasing for increased resistance and decreased inductance.

Figure 4.15 shows that for 96 mH inductance the dv/dt remains slightly around at 5000 to 12000 V/ms but breakdown voltage varies largely in range of 300 volts for different values of resistance. Further as inductance value decreases to 44 mH, the dv/dt value found to have slightly less range of value between 15000 to 29000 V/ms and breakdown voltage remains same to 300 volts. For lowest inductance value of 12 mH, dv/dt increases in large range from 17500 to 111000 V/ms but breakdown voltage range being largest value of 575 volts.

Overall, the breakdown voltage is found highest for 4.7 Ω resistance values followed by 47 Ω and 280 Ω respectively. The dv/dt value keep increasing for increased resistance and decreased inductance.

4.3.3 For 40 bar pressure

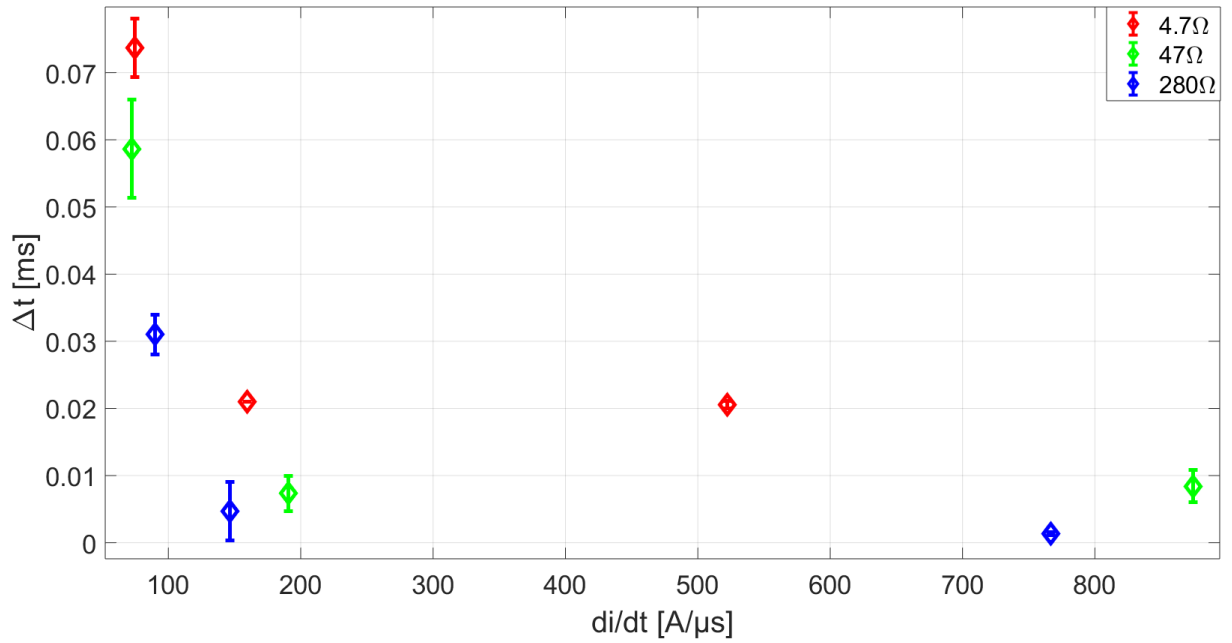


Figure 4.16: Delay in restriking (Δt) versus rate of change of current (di/dt) just before current zero at 40 bar pressure.

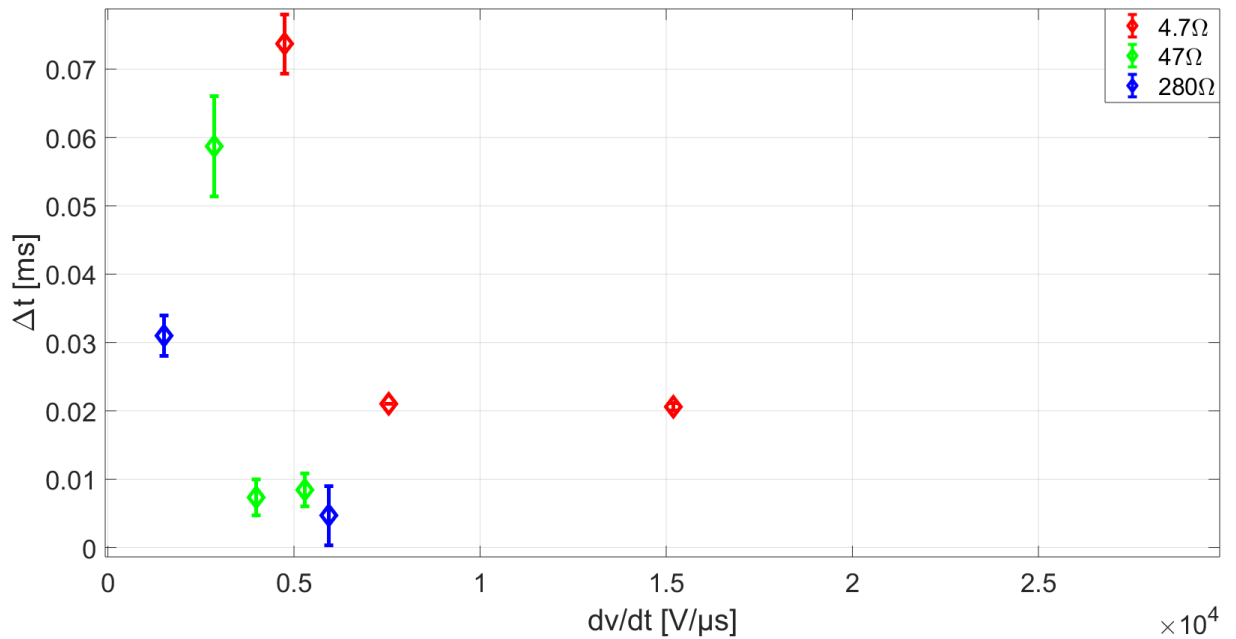


Figure 4.17: Delay in restriking (Δt) versus rate of change of TRV (dv/dt) after current zero at 40 bar pressure.

Figure 4.16 shows that for 96 mH inductance the di/dt remains slightly between 50 to 80 A/ms but Δt varies largely between 0.03 to 0.075 milliseconds for different values of resistance. Higher the R , lower the Δt . This is expected as high R will impose steep IRRV and the restrike occurs earlier. This can be shown clearly from above figures 4.16 and 4.17. Further as inductance value decreases to 44 mH, the di/dt differs marginally between 150 to 200 A/ms and Δt decreases to range between 0.005 to 0.021 milliseconds. For lowest inductance value of 12 mH, di/dt increases in large range from 525 to 875 A/ms but Δt varies marginally between 0.001 to 0.02 milliseconds.

Overall, the time delay to restrike (Δt) is highest for 4.7 Ω resistance values followed by 47 Ω and 280 Ω respectively. A common trend of decreased Δt and high increase di/dt is observed for increased resistance and decreased inductance.

In the figure 4.17, it can be shown that high dv/dt results in low Δt . The Δt is highest for 4.7 Ω resistance values followed by 47 Ω and 280 Ω respectively. The dv/dt range 4.7 Ω is found to be in varying slightly. For 47 Ω it is found to be decreasing and almost constant value. For 280 Ω , its range is found to be largest. Here a common trend of decreased Δt , with increase dv/dt is observed.

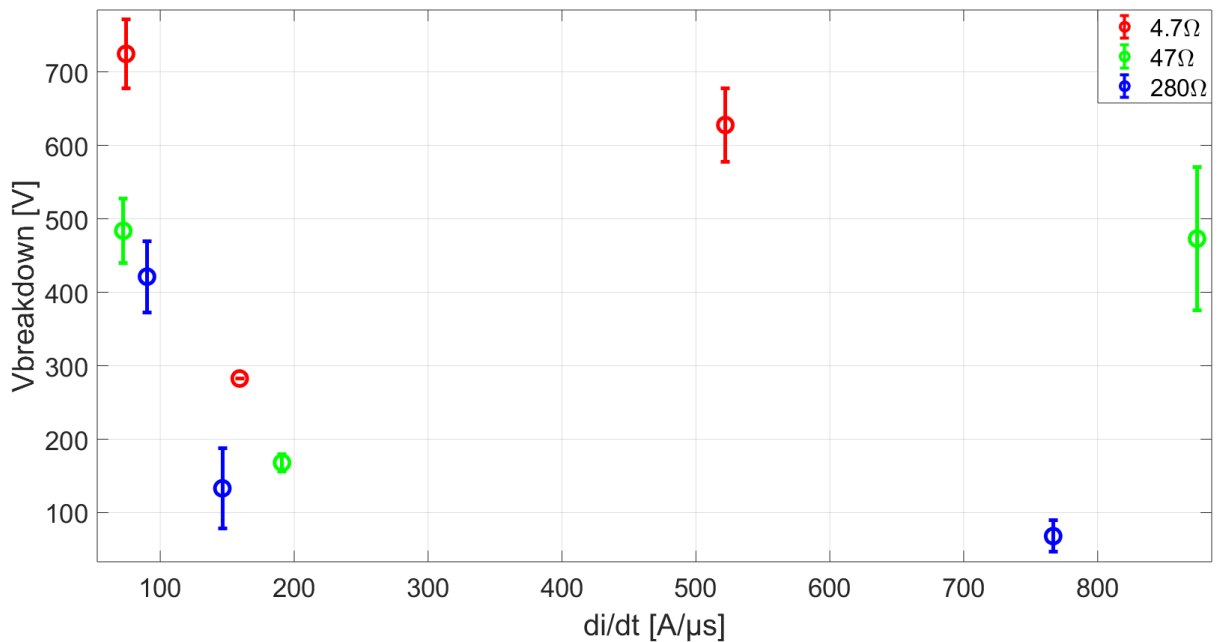


Figure 4.18: Breakdown voltage versus rate of change of current (di/dt) just before current zero at 40 bar pressure.

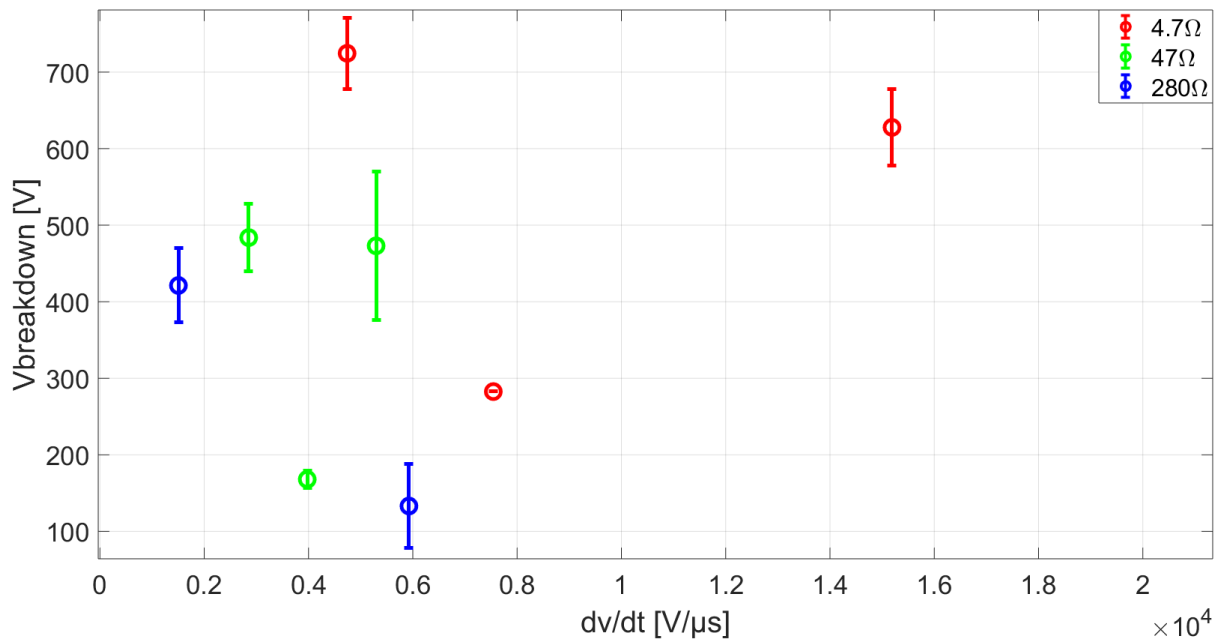


Figure 4.19: Breakdown voltage versus rate of change of TRV (dv/dt) after current zero at 40 bar pressure.

Figure 4.18 shows that for 96 mH inductance the di/dt remains slightly around at 90 A/ms but breakdown voltage varies largely in range of 300 volts for different values of resistance. Further as inductance value decreases to 44 mH, the di/dt value found to have increased value between 150 to 200 A/ms and breakdown voltage range decreases to 150 volts. For lowest inductance value of 12 mH, di/dt increases in large range from 525 to 875 A/ms but breakdown voltage range being largest value of 525 volts.

Overall, the breakdown voltage is found highest for 4.7 Ω resistance values followed by 47 Ω and 280 Ω respectively. The di/dt value keep increasing for increased resistance and decreased inductance.

Figure 4.19 shows that for 96 mH inductance the dv/dt remains slightly around at 10000 to 12000 V/ms but breakdown voltage varies largely in range of 300 volts for different values of resistance. Further as inductance value decreases to 44 mH, the dv/dt value found to have slightly less range of value between 10000 to 10500 V/ms and breakdown voltage range decreases to 150 volts. For lowest inductance value of 12 mH, dv/dt increases in large range from 12000 to 260000 V/ms but breakdown voltage range being largest value of 525 volts.

Overall, the breakdown voltage is found highest for 4.7 Ω resistance values followed by 47 Ω and

280 Ω respectively. The dv/dt value keep increasing for increased resistance and decreased inductance.

4.3.4 For 1, 20 and 40 bar pressure

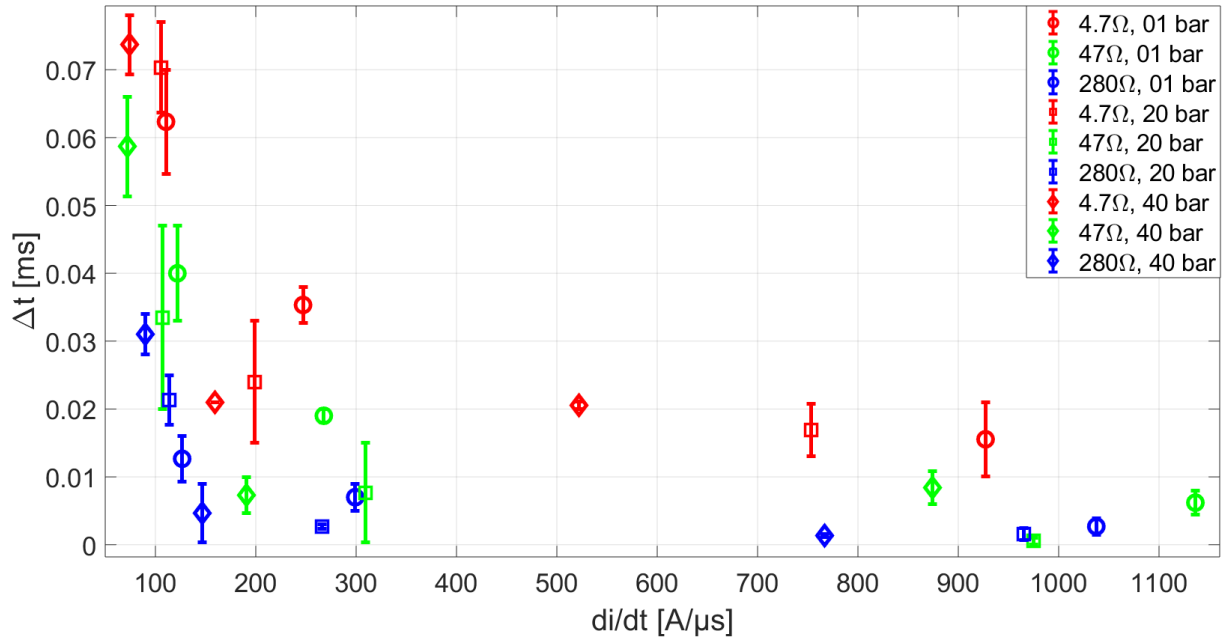


Figure 4.20: Delay in restriking (Δt) versus rate of change of current (di/dt) just before current zero 1, 20 and 40 bar pressure.

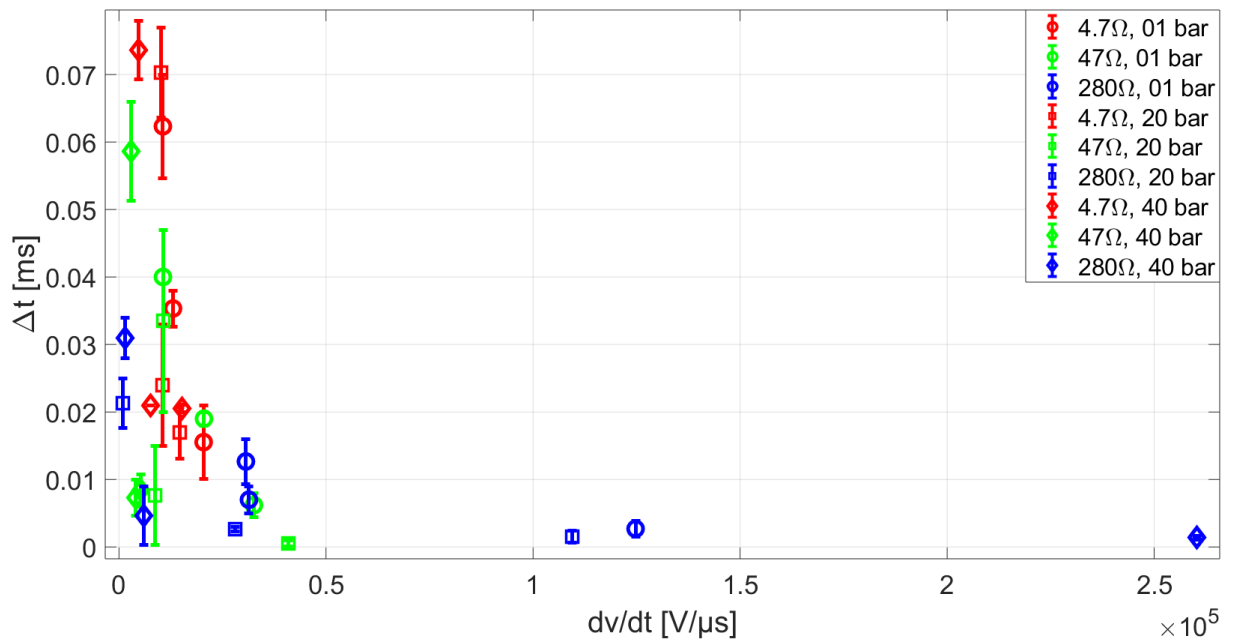


Figure 4.21: Delay in restriking (Δt) versus rate of change of TRV (dv/dt) after current zero at 1, 20 and 40 pressure.

Figure 4.20 shows that, higher the R , lower the Δt . This is expected as high R will impose steep IRRV and the restriking occurs earlier. This can be shown clearly from above figures 4.20 and 4.21. The time delay to restriking (Δt) is highest for 4.7Ω resistance values followed by 47Ω and 280Ω respectively. A common trend of decreased Δt and high increase di/dt is observed for increased resistance and decreased inductance.

In the figure 4.21, it can be shown that high dv/dt results in low Δt . For all the pressure values a common trend of decreased Δt , with increase dv/dt is observed.

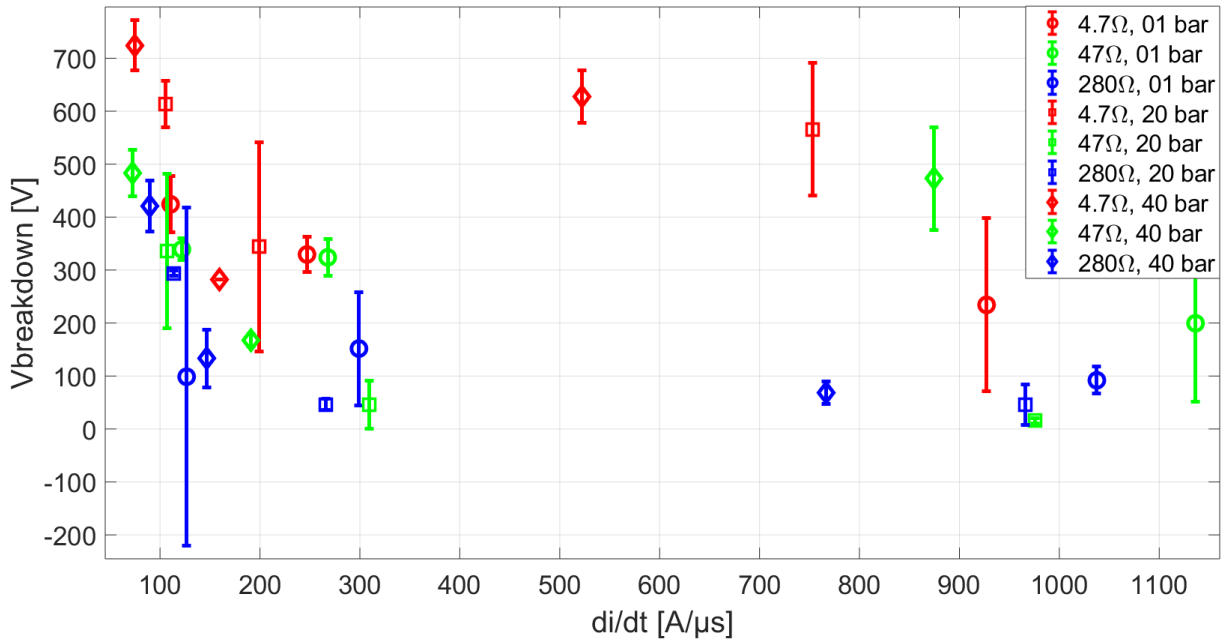


Figure 4.22: Breakdown voltage versus rate of change of current (di/dt) just before current zero at 1, 20 and 40 bar pressure.

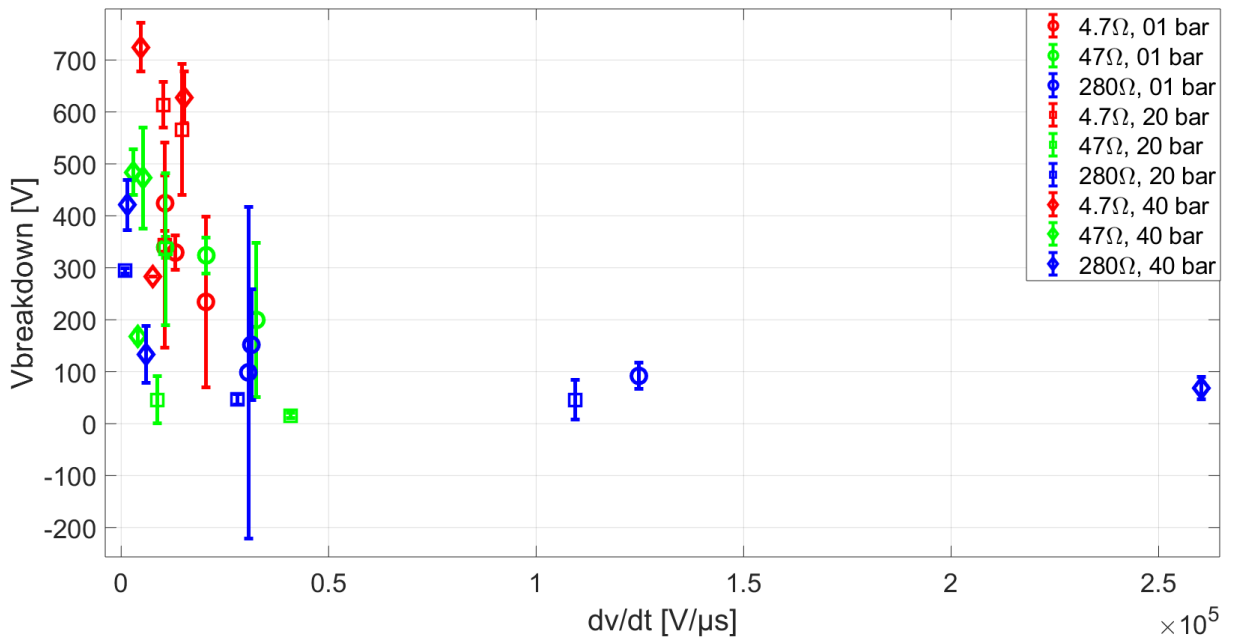


Figure 4.23: Breakdown voltage versus rate of change of TRV (dv/dt) after current zero at 1, 20 and 40 bar pressure.

The figure 4.22 shows that, the breakdown voltage is found highest for 4.7 Ω resistance values

followed by 47 Ω and 280 Ω respectively. The di/dt value keep increasing for increased resistance and decreased inductance.

The figure 4.23 shows that, the dv/dt value keep increasing for increased resistance and decreased inductance. For all the pressure values a common trend of decreased breakdown voltage with increase in dv/dt is observed.

4.4 Discussion

The initiation of thermal re-ignition depends upon rate of rise (dv/dt) of TRV soon after current zero and the time taken to re-ignite the arc is considered as the main parameter to characterise the post arc thermal reignition at different pressure levels. It has been concluded from the results that, for different filing pressures, no strong connection of delay time is observed. For different pressures tested, a common trend of decreased Δt and high increase di/dt and dv/dt is observed for increased dv/dt and decreased di/dt .

The observation from the results were expected, as presented in simulation part in the section 3.1. The increase in resistance values the rate of rise of TRV increases and increase in inductance decreases the di/dt slope.

The experimental circuit have no control on the delay time to post arc voltage applied. Also, there is no active cooling mechanism present might be one of the reason which limits us from expecting improved restrike performance in free burning arc at SC state. The data recorded from the experiment have the error margin added from voltage and current probes and accuracy of the signal transmitters and receivers.

Chapter 5

Conclusions

The objective of this thesis was to study the post arc dielectric recovery characteristics of free burning arc at high pressure filled nitrogen chamber. The experiment is conducted at various pressure levels for different di/dt and dv/dt . Based on the experimental findings following conclusions can be drawn.

1. At atmospheric pressure, a high dv/dt facilitates the reignition earlier, which is expected.
2. At atmospheric pressure, a high di/dt causes faster reignition.
3. At high filling pressure, this general trend of dependency on di/dt and dv/dt is also observed.
4. When compared to different filling pressures, no strong correlation of delay time to re-strike and filling pressure was observed.

5.1 Recommendations for Further Work

There is scope for further research or study for this thesis topic. Some of such recommendations can be classified as:

- Use of more practical circuit using Triggering and time delay units to control the delay time to applying voltage pulse for further precise study of re-strike possibilities.
- Use of high speed camera to study post arc re-ignition and arcing channel.
- Use of high value capacitors in the circuit can produce high current amplitude. Thus post arc current behaviour can be studied for practical switchgear operational voltage and current values.
- Use of active cooling mechanism, such as puffer or self blast techniques on the dependency of filling pressure can be explored.

Bibliography

- [1] Baard Jonas Wigestrands. Arve Skjetne. Pressure compensator for a subsea device, May 5 2015. URL <http://www.google.it/patents/US4741207>. US Patent 9,038,433 B2.
- [2] T.Rak. SF_6 free hv gis and breakers, January 1 2017.
- [3] I. Spiliopoulos, G. Berger, E. Marode, S. W. Rowe, G. Bernard, and David R. James. *Dielectric Recovery of SF_6 During the Post-Arc Phase*. Springer US, Boston, MA, 1994.
- [4] Chen Degui, Li Xingwen, and Dai Ruicheng. *Measurement of the dielectric recovery strength and reignition of AC contactors*, 2004. URL <http://id.ndl.go.jp/bib/7153486>.
- [5] Hiroyuki Tanoue, Tomohiro Furusato, Takahiro Imamichi, Miyuki Ota, Sunao Katsuki, and Hidenori Akiyama. Dielectric recovery mechanism of pressurized carbon dioxide at liquid and supercritical phases. *Japanese Journal of Applied Physics*, 54(9):096102, 2015. URL <http://stacks.iop.org/1347-4065/54/i=9/a=096102>.
- [6] J Zhang, A H Markosyan, M Seeger, E M van Veldhuizen, E J M van Heesch, and U Ebert. Numerical and experimental investigation of dielectric recovery in supercritical n_2 . *Plasma Sources Science and Technology*, 24(2):025008, 2015. URL <http://stacks.iop.org/0963-0252/24/i=2/a=025008>.
- [7] F Abid, K. Niayesh, E. Jonsson, N. S. Støa-Aanensen, and M. Runde. Arc voltage characteristics in ultrahigh-pressure nitrogen including supercritical region. *IEEE Transactions on Plasma Science*, 46(1):187–193, Jan 2018. ISSN 0093-3813. doi: 10.1109/TPS.2017.2778800.
- [8] A. Karimi and K. Niayesh. A simple evaluation method of the thermal interruption limit of power circuit breakers. *Electrical Engineering*, 90(8):523–528, Feb 2009. ISSN 1432-0487. doi: 10.1007/s00202-008-0103-9. URL <https://doi.org/10.1007/s00202-008-0103-9>.
- [9] K. Niayesh and M. Runde. *Power Switching Components*. Springer, Gewerbestrasse 11, 6330 Cham, Switzerland, 2017.

- [10] E. Schade and K. Ragaller. Dielectric recovery of an axially blown sf_6 -arc after current zero: part i-experimental investigations. *IEEE Transactions on Plasma Science*, 10(3):141–153, Sept 1982. ISSN 0093-3813. doi: 10.1109/TPS.1982.4316161.
- [11] H. Edels and Y. Ettinger. Arc interruption and thermal reignition. *Proceedings of the IEE - Part A: Power Engineering*, 109(43):89–98, February 1962. ISSN 0369-8882. doi: 10.1049/pi-a.1962.0074.
- [12] J J Lowke. Simple theory of free-burning arcs. *Journal of Physics D: Applied Physics*, 12(11): 1873, 1979. URL <http://stacks.iop.org/0022-3727/12/i=11/a=016>.
- [13] L M Vasilyak, S V Kostyuchenko, N N Kudryavtsev, and I V Filyugin. Fast ionisation waves under electrical breakdown conditions. *Physics-Uspekhi*, 37(3):247, 1994. URL <http://stacks.iop.org/1063-7869/37/i=3/a=R02>.
- [14] E. J. M. van Heesch, J. Zhang, T. Namihira, A. H. Markosyan, F. J. C. M. Beckers, T. Huiskamp, W. F. L. M. Hoeben, A. J. M. Pemen, and U. Ebert. Supercritical fluids for high-power switching. In *2014 IEEE International Power Modulator and High Voltage Conference (IPMHVC)*, pages 126–129, June 2014. doi: 10.1109/IPMHVC.2014.7287224.
- [15] Andrea Capuzzo, Massimo E. Maffei, and Andrea Occhipinti. Supercritical fluid extraction of plant flavors and fragrances. *Molecules*, 18(6):7194–7238, 2013. ISSN 1420-3049. URL <http://www.mdpi.com/1420-3049/18/6/7194>.
- [16] Daniel Banuti, Muralikrishna Raju, Peter Ma, Matthias Ihme, and Jean-Pierre Hickey. *Seven questions about supercritical fluids-towards a new fluid state diagram*, 01 2017.
- [17] J. Zhang. *Supercritical fluids for high power switching*. PhD thesis, TUE : Department of Electrical Engineering, 2015.
- [18] Tomoyuki Nakano, Yasunori Tanaka, K Murai, Y Uesugi, T Ishijima, K Tomita, K Suzuki, and T Shinkai. Thermal re-ignition processes of switching arcs with various gas-blast using voltage application highly controlled by power semiconductors. *Journal of Physics D: Applied Physics*, 51(21):215202, 2018. URL <http://stacks.iop.org/0022-3727/51/i=21/a=215202>.
- [19] Tsuyohito Ito and Kazuo Terashima. Generation of micrometer-scale discharge in a supercritical fluid environment. *Applied Physics Letters*, 80(16):2854–2856, 2002. doi: 10.1063/1.1470695. URL <https://doi.org/10.1063/1.1470695>.
- [20] J. Zhang, B. van Heesch, F. Beckers, T. Huiskamp, and G. Pemen. Breakdown voltage and recovery rate estimation of a supercritical nitrogen plasma switch. *IEEE Transactions on Plasma Science*, 42(2):376–383, Feb 2014. ISSN 0093-3813. doi: 10.1109/TPS.2013.2294756.

- [21] Z. B. Yang, S. H. R. Hosseini, T. Kiyan, S. Gnapowski, and H. Akiyama. Post-breakdown dielectric recovery characteristics of high-pressure liquid CO_2 including supercritical phase. *IEEE Transactions on Dielectrics and Electrical Insulation*, 21(3):1089–1094, June 2014. ISSN 1070-9878. doi: 10.1109/TDEI.2014.6832252.
- [22] Karl Schoenbach, Juergen Kolb, Shu Xiao, Sunao Katsuki, Yasushi Minamitani, and Ravindra Joshi. Electrical breakdown of water in microgaps. *Plasma Sources Science and Technology*, 17(2):024010, 2008. URL <http://stacks.iop.org/0963-0252/17/i=2/a=024010>.
- [23] *P6015A Instruction Manual*. Tektronix, Beaverton, OR 97077 USA, 070-8223-05 edition, 2002.
- [24] *HVP-15HF Instruction Manual*. Pintek, tinse0031s4, rev.01 edition, .
- [25] *LTX-5510R operating instructions*. Terahertz Technologies Inc, 169 Clear Road, Oriskany, NY, 2011.
- [26] *Mixed Signal Oscilloscopes, MSO2000 Series, DPO2000 Series Data Sheet*. Tektronix, 3gw-22048-1 edition, 2009.
- [27] Nicholas J. Tate, Chris Brunsdon, Martin Charlton, A. Stewart Fotheringham, and Claire H. Jarvis. Smoothing/filtering lidar digital surface models. experiments with loess regression and discrete wavelets. *Journal of Geographical Systems*, 7(3):273–290, Dec 2005. ISSN 1435-5949. doi: 10.1007/s10109-005-0007-4. URL <https://doi.org/10.1007/s10109-005-0007-4>.